The Composition of Magmatic-Hydrothermal Fluids in Barren and Mineralized Intrusions

Journal Article

Author(s):
Audétat, Andreas; Pettke, Thomas; Heinrich, Christoph A. (iD); Bodnar, Robert J.

The composition of magmatic-hydrothermal fluids in barren versus mineralized intrusions

Andreas Audétat[1], Thomas Pettke[2], Christoph A. Heinrich[2,3], Robert J. Bodnar[4]

[1]*Bayerisches Geoinstitut, University of Bayreuth, 95440 Bayreuth, Germany*
[2]*Isotope Geochemistry and Mineral Resources, Department of Earth Sciences, Swiss Federal Institute of Technology, ETH Zentrum, Clausiusstrasse 25, 8092 Zürich, Switzerland*
[3]*Faculty of Mathematics and Natural Sciences, University of Zürich*
[4]*Department of Geosciences, 4044 Derring Hall, Virginia Tech, Blacksburg, VA 24061, U.S.A.*

Abstract

This paper addresses the question of whether or not there are fundamental differences in the composition of magmatic-hydrothermal fluids in barren versus variably mineralized systems, and if so, at which stage of magmatic-hydrothermal evolution the differences were generated. Combining microthermometry and laser-ablation microanalysis, we studied high-temperature, pre-mineralization fluid inclusions in three barren granites, one Sn-W-mineralized granite, one porphyry Cu-mineralized intrusion, one porphyry Mo-mineralized intrusion, and one Th-U-REE-mineralized granite, and compared the results with published data from 10 other intrusive systems. Many of the fluid inclusions are paragenetically associated with melt inclusions, providing direct insights into the stage at which metals were transferred from the crystallizing magma into the exsolving aqueous fluids.

In 10 out of 14 magma systems in which the physical and compositional properties of the magmatic fluid(s) could be determined, the exsolved aqueous fluid was single-phase and of relatively low salinity (2-13 wt% $NaCl_{equiv}$; average 5 wt% $NaCl_{equiv}$), confirming predictions based on indirect evidence and observations made in earlier studies. Furthermore, in magmas that crystallized at low pressure (< 1.3 kbar), the salinity of the magmatic fluid increased with increasing degree of crystallization, whereas in magmas that crystallized at higher pressure (>1.3 kbar) the opposite behavior occurred, as predicted by published numerical models of aqueous fluid-saturated magma crystallization. During the transition from magmatic to subsolidus conditions, both pressure and temperature within and adjacent to intrusions decreased, leading to widespread vapor-brine immiscibility. Due to the low salinity of the single-phase parent fluid the two-phase field generally was entered from the vapor side, resulting in condensation of subordinate amounts of brine from the low-density bulk fluid. If the transition from single- to two-phase aqueous fluid occurred in locally closed systems one can use the compositions of vapor and brine in subsolidus boiling assemblages to calculate the composition of the bulk fluid. This method was applied to those occurrences in which no single-phase parent fluid was found (i.e., where the earliest aqueous fluid found was already in the two-phase field).

The metal content of the least fractionated low-salinity fluids at each location correlates positively with the type and amount of mineralization in the associated intrusions, with high Cu concentrations being observed in fluid related to porphyry Cu deposits, high Sn and W concentrations in fluids related to Sn-W mineralization, and high Ce concentrations

in fluids related to REE mineralization. The earliest fluids in barren intrusions are comparatively metal poor, except for two cases in which certain metal concentrations are as high as in mineralized systems. A significant portion of the geochemical signature of barren versus mineralized intrusions was thus inherited from earlier stages in the development of these magma systems. In the case of Mo, Sn, W and Ce, the correlation between fluid composition and type and amount of mineralization is more distinct in high-temperature brines than in the least fractionated low-salinity fluids. This, together with other lines of evidence, suggests that brine condensates play a central role in the formation of Sn, W, Mo and REE deposits. In the case of porphyry Cu (-Au) systems it appears more likely that the greater proportion of metal precipitated from the vapor phase, although brines may have played a significant role as well.

1. Introduction

Magmatic-hydrothermal ore deposits show a close association with igneous intrusions and evidence for metal transport by hydrothermal fluids. Such deposits are our main source of Cu, Mo, Sn, W and Bi, and a significant source of Au, Ag, Pb and Zn (Kesler, 1994). Styles of mineralization vary from vein, skarn, and greisen to porphyry type. Models for the genesis of these deposits – in particular the porphyry types – have evolved significantly over time, from early days when the intrusions were regarded as the source of all components of the ore deposits (e.g., Lindgren, 1905; Bowen, 1933; Emmons, 1933; Fenner, 1933), to a time when most researchers regarded the intrusions only as heat sources, driving large convection cells of meteoric water which leached metals out of the surrounding country rocks (e.g., Sheppard et al., 1971; Taylor, 1974; Cathles, 1981; Norton, 1982), and finally back to a broader acceptance of the original view (e.g., Burnham, 1967; Nielsen, 1968; Lowell and Guilbert, 1970; Roedder, 1971; Henley and McNabb, 1978; Cline and Bodnar, 1991; Bodnar, 1995). Reviews by Hedenquist and Lowenstern (1994) and Hedenquist and Richards (1998) have traced this evolution of understanding.

This paper focuses on the question of whether fundamental differences exist between barren and mineralized intrusions, and if so, whether these differences are reflected in the composition of the magmatic-hydrothermal fluids. In the first section we examine two examples of mostly barren intrusions (the Rito del Medio Pluton, New Mexico, and the Stronghold Granite, New Mexico) and four examples of mineralized intrusions (the porphyry Cu mineralized Santa Rita deposit, New Mexico, USA; the porphyry Mo mineralized Cave Peak deposit, Texas, USA; the Sn-W-base metal mineralized Mole Granite, New South Wales, Australia, and the REE-mineralized Capitan Pluton, New Mexico, USA). The aqueous fluids that are most likely to have exsolved from the crystallizing magmas and were ultimately responsible for mineralization are characterized. Our observations are then used along with published data from three other barren intrusions (Baveno, Italy; Cuasso al Monte, Italy; Mt. Malosa, Malawi), five other porphyry Cu deposits (Bajo de la Alumbrera, Argentina; Bingham, Utah, USA; Butte, Montana, USA; Grasberg, Indonesia; El Teniente, Chile), another porphyry Mo deposit (Questa, New Mexico, USA) and another Sn deposit (Ehrenfriedersdorf, Germany) to demonstrate that the mineralization potential of a given intrusion is in part reflected by the composition of the aqueous fluid(s) exsolved at the magmatic stage, and is in part influenced by the subsequent fluid evolution after complete magma solidification.

2. Methods

In order to find fluid inclusions that are both well preserved and have been trapped at high temperatures (i.e., as close as possible to magma solidus conditions), we focused our search on crystals that grew in miarolitic cavities or in open spaces within high-temperature veins in porphyry deposits. Samples containing fluid and melt inclusions

that were trapped unambiguously at the same time were found at six localities. In the other localities high-temperature, pre-mineralization fluid inclusions were identified by a combination of petrographic mapping and microthermometry. In practice, numerous specimens had to be collected and examined to find one sample in which the fluid inclusions are both well preserved (see e.g., Audétat and Günther, 1999, for characteristics of less well-preserved inclusions) and representative of pre-mineralization fluids.

Fluid inclusion assemblages (Goldstein and Reynolds, 1994) were studied with a standard petrographic microscope, a Linkam THMSG600 heating/freezing stage, and a custom-built Linkam heating stage able to attain temperatures up to 1000 °C. This study allowed determination of the physical state of the fluid (single-phase versus two-phase), the type of fluid system ($NaCl$-H_2O, other major cations, presence/absence of condensed gases such as CO_2), fluid salinity and fluid density, and – in case of fluid entrapment in the two-phase field – pressure and temperature of entrapment. In the context of fluids and fluid inclusions the following terminology is used in this manuscript: the term "fluid" is used for a mobile phase dominated by volatile constituents of the H-O-C-N-S system with variable concentrations of dissolved components such as chloride salts, "single-phase fluid" is used for a fluid of any composition and density plotting above the two-phase (liquid + vapor) surface (the latter being equivalent to a solvus), and "two-phase field" is used to describe the P-T-X-region below this solvus. "Vapor" is used for an H_2O-rich, salt-bearing (± CO_2 and other volatiles) fluid with a density below the critical density of a solution of that particular composition, "liquid" for an H_2O-rich, salt-bearing fluid with a density above the critical density of a solution of that particular composition, and "brine" for a liquid with >26 wt% $NaCl_{equiv}$ (i.e., salt-saturated at room temperature). The term "boiling assemblage" is used for assemblages of vapor and brine or liquid inclusions that formed at the same time (i.e., due to trapping of a two-phase fluid). In this manuscript, the term "magmatic fluid" is a fluid that was trapped during the magmatic stage, i.e., at pressure-temperature conditions on or above the H_2O-saturated solidus of the magma. In contrast to this, a fluid trapped at subsolidus conditions is called a "subsolidus fluid".

Whenever possible, fluid salinities were determined for all inclusions that subsequently were analyzed by laser-ablation inductively coupled plasma-mass spectrometry (LA-ICP-MS). This is particularly important for vapor inclusions that formed in the two-phase field, as they commonly contain small amounts of brine trapped along with the vapor (Bodnar et al., 1985). However, final melting temperatures of ice and clathrates in low-density vapor inclusions commonly are exceedingly difficult to measure, and in some cases it was not possible to obtain microthermometric data from the same inclusion that was also analyzed by LA-ICP-MS. Homogenization temperatures usually were determined after LA-ICP-MS analysis, using inclusions that were situated on the same trail as those analyzed.

LA-ICP-MS analyses of fluid and melt inclusions were performed at the Institute of Isotope Geology and Mineral Resources at ETH Zürich and at the Bayerisches Geoinstitut in Bayreuth, using an 193nm ArF Excimer Laser System (Geolas M from Coherent / Lambda Physik) attached to either a Perkin Elmer Elan 6100 (Zürich) or a Perkin Elmer Elan DRC-e (Bayreuth) quadrupole mass spectrometer. Details about the instrumentation and quantification procedure for fluid inclusions can be found in Günther et al. (1998) and Heinrich et al. (2003). Total uncertainties in *absolute* element concentrations in fluid inclusions are about 20 percent (relative) in most cases, but might reach 50 percent in inclusions in which Na is not the dominant cation. Uncertainties in *relative* element concentrations are about 5 to10 percent and reflect mostly uncertainties in the reference values of element concentrations in the external standard material (NIST SRM610 in our case). For very short signals close to the detection limit the uncertainty in relative element concentrations can reach several tens of percent (Pettke et al., 2000).

Melt inclusions in the Stronghold Granite are completely crystallized, as is typical of melt inclusions in plutonic rocks (Bodnar and Student, 2006). For LA-ICP-MS analysis entire melt inclusions were drilled out of the host quartz without prior homogenization, and original melt compositions were calculated using procedures described in Halter et al. (2002a) and Pettke (2006). Internal standardization was based on Al, the concentration of which is well constrained at 12.8 ± 0.5 wt percent Al_2O_3 by whole-rock values and microprobe analyses of two rehomogenized melt inclusions. Overall uncertainties in the calculated absolute element concentrations in melt inclusions are considered to be less than 15 percent relative.

2.1. Samples from miarolitic cavities

Many of the samples described in this paper were collected from miarolitic cavities. Miarolitic cavities (or miaroles) are voids in plutonic rocks that are interpreted to have formed by accumulation and migration of fluid at the magmatic stage (e.g., Candela, 1995). They vary in size from millimeters to several meters, are crystal-lined (quartz, orthoclase ± other minerals), and commonly are rimmed by a zone of granophyric to pegmatitic texture. A study of miarolitic cavities from two barren granites in New Mexico (Audétat and Pettke, 2003) revealed that they formed at high degrees of magma crystallization (≥90 vol% crystallinity), as implied by the Cs content of various generations of melt inclusions analyzed from these plutons. As shown by these authors, Cs behaves incompatibly in granitic magmas both under fluid-undersaturated and fluid-saturated conditions if the salinity of the bulk fluid is low (≤ 10 wt% $NaCl_{equiv}$), leading to an exponential increase in the Cs content of the residual melt with increasing degree of magma crystallization (Fig. 1a). Compared to the large range of absolute Cs concentrations observed in natural melt inclusions (commonly spanning several orders of magnitude within a single intrusion), fluid/melt partition coefficients determined on natural assemblages of coexisting fluid and melt inclusions are relatively constant. Thus, increasing Cs concentrations in residual melts are accompanied by increasing Cs concentrations in the exsolving fluids. The Cs content of magmatic, single-phase fluids analyzed from a given intrusion can thus be used to place the fluids into a relative sequence of melt fractionation. In this sense, the term "fractionated" will be used interchangeably for both melts and magmatic fluids. Following this reasoning we plotted fluid compositional data generally against the Cs content of the fluid.

It should be noted that the amount of fluid that is exsolved per mass unit of crystallizing magma remains approximately constant, whereas the concentration of Cs in the residual melt and associated fluid increases exponentially with increasing magma crystallization. Consequently, the amount of exsolved fluid of a given Cs concentration decreases exponentially with increasing degree of crystallinity (Fig. 1b). In other words, when looking at single-phase magmatic fluids trapped at various stages in a crystallizing pluton one can expect that the fluids with high Cs content were much less abundant than those with low Cs content. Because miarolitic cavities (and euhedral crystals contained in them) may have formed significantly later than the time at which fluid saturation was reached in a given magma chamber, it is possible that fluid inclusions in miarolitic quartz may be different from the average fluid exsolved from this magma. However, as will be shown below, there is strong evidence that the earliest fluids trapped in miarolitic quartz are representative of the mineralizing fluids – whether or not they are representative of the average fluid exsolved from the magma.
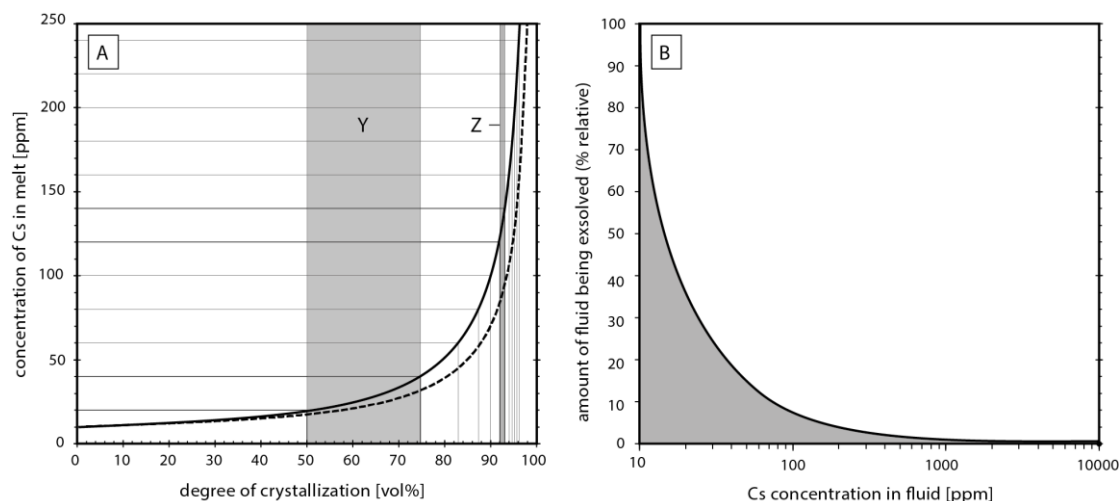
Figure 1. A. Model calculation showing the evolution of Cs in the residual melt of a crystallizing magma as a function of the degree of crystallization, with the starting Cs concentration set arbitrarily to 10 ppm. This relationship is used to monitor melt fractionation. The thick, solid line represents the fractionation curve followed if Cs behaves 100 % incompatibly (i.e., if no Cs is incorporated in the crystallizing minerals and no fluid exsolves). The dashed line corresponds to the fractionation curve calculated for open-system, fluid-saturated fractional crystallization in the Rito del Medio Pluton (Audétat and Pettke, 2003), which is thought to be representative of many granitic systems. Note that with increasing degree of crystallization the amount of fluid exsolved per mass unit magma stays approximately constant, whereas the Cs concentration in the melt increases exponentially. Hence, the amount of fluid exsolved at a given Cs concentration decreases exponentially with increasing crystallinity. For example, the amount of fluid exsolved from melts containing 20-40 ppm Cs (represented by the gray box labeled Y), is more than 20 time larger than the amount of fluid exsolved from melts containing 120-140 ppm Cs (represented by gray box labeled Z). A similar relationship holds if the y-axis of the diagram is replaced by Cs concentration in the fluid, because the fluid/melt partition coefficient of Cs stays relatively constant compared to the large change in absolute Cs concentrations. **B**. Plot showing the amount of exsolved fluid as a function of its Cs content, assuming a constant fluid/melt partition coefficient of 1 and 100 % incompatibility of Cs in the crystallizing minerals. Note that the amount of exsolved fluid decreases exponentially even though the Cs concentration in the fluid is plotted on a logarithmic scale.

3. Compositional Evolution of Magmatic-hydrothermal Fluids

3.1. Stronghold Granite: Minor Zn-Pb-Cu mineralization

The 27-28 Ma Stronghold granite in southeast Arizona is an alkalic granite, containing 25 to 35 volume percent quartz, 30 to 40 percent each of plagioclase and potassic feldspar, and 1 to 4 percent biotite (Gilluly, 1956; Drewes, 1987). Accessory minerals include magnetite, apatite, zircon, allanite, fluorite, as well as rare muscovite, sphene and rutile. The intrusion crops out over an area of ~60 km² (plus an estimated subsurface area of ~10 km²), and has a relief of 580 m. The surrounding country rocks consist of folded and thrusted Precambrian amphibolites, granodiorite and schists, which are overlain by Permian limestone and Cretaceous shales and siltstones. Three textural facies have been distinguished within the intrusion: a coarse-grained facies that makes up the main mass of the stock (68-74 wt% SiO_2), a porphyritic border facies (no whole-rock analysis available), and an aplitic facies (77 wt% SiO_2). Rhyolitic dikes containing ~25 volume percent quartz plus feldspar phenocrysts cut the granite and overlying country rocks in conspicuous swarms trending northwest. Petrographic and chemical characteristics as well as crosscutting relationships (many dikes cut the granite, but not the adjacent country rocks) suggest that these dikes and the granite are consanguineous. About 60 small mines and workings are known in the vicinity of the Stronghold granite (Keith, 1973; Kreidler, 1982). Most of them are small manto or chimney-type deposits within Permian limestone close to the granite contact. Major commodities are Zn, Pb and/or Cu with minor amounts of Ag, Au and W. Total production until 1970 was about 69,000 t (metric tons) of ore containing 4200 t Zn, 900 t Cu, 125 t of Pb, 4.6 t Ag, 10 kg Au, 2 t scheelite concentrate and 70 t barite (Kreidler, 1982). Even if all this ore was won from a

single mine only, the tonnage of Zn would indicate that this is at most a small deposit – the tonnages of all other elements are significantly below those of the smallest deposit size defined in the mining section of GIS Central Europe to qualify as a deposit (http://giseurope.brgm.fr/). Relative to the large size of the pluton this amount of known ore is certainly very small (Table 1).

Table 1. Phyiscal and chemical properties of high-temperature fluids from various styles of ore deposits and barren intrusive systems

Mineralization	Size[1]	Locality	Sample type[2]	Single-phase	Two-phase	MI[3]	NaCl$_{equiv}$ (wt%)	T (°C)	P (bar)	References
barren	-	Rito del Medio	M	x		x	4.5 - 7.5	700-720	1100-1300	(2)
barren	-	Canada Pinabete	M	x		x	2.6 - 4.8	600-720	950-1300	(2)
barren[4]	-	Baveno	M	x		x	5,9	650-670	ca. 1900	(15)
barren[4]	-	Cuasso al Monte	M		x	x	? / 53-69	690-720	800-1000	(15)
barren[4]	-	Mt. Malosa	M		x	x	7-13 / 32-35	670-700	1150-1300	(15)
(Zn-Pb-Cu)	S	Stronghold	M	x		x	3.1 - 6.2	670-700	1500-1800	(1)
Cu (Mo-Au)	L	Santa Rita	M		x	x	20 / 33	700-740	1200-1300	(1)
Cu-Au-Mo	L	Alumbrera	V	(?)		x	1-5 / 37-68	>600	700-1200	(3)
Cu-Au (Mo-Ag-Pb-Zn)	VL	Bingham	V	x			2.0-7.0	>550	900	(4), (5), (6)
Cu (Mo-Ag-Zn-Au)	VL	Butte	V	x			2.5-2.7	550-700	2000-3000	(7)
Cu-Au (Ag)	VL	Grasberg	V		x		4-10 / 68-76	600-680	?	(6), (8), (9)
Cu (Mo)	VL	El Teniente	V	x			12-13	?	?	(16)
Mo-Nb (Cu-W)	VL	Cave Peak	M		x		3.1 / 38	600	800	(1)
Mo	L	Questa	M/V	x			2.0-7.6	?	?	(11)
Sn-W (Cu-Ag-Pb-Zn)	L	Mole Granite	M	x		x	3.1 - 8.0	710-730	950-1000	(1), (12), (13), (14)
Sn (W)	L	Ehrenfriedersdorf	M	x		x	7.0 - 8.5	680-710	ca. 1000	(15)
(Th-U-REE)	-	Capitan Mt.	P		x	x	2.2 / 63	630-690	600	(1)

[1] Deposit size classification scheme according to the mining section of GIS Central Europe (http://giseurope.brgm.fr/); S-small, L-large, VL-very large; size estimate according to data in Kreidler, 1982 (Stronghold Granite), Plimer et al., 1995 (Mole Granite), Baumann et al., 2000 (Ehrenfriedersdorf), and Mutschler et al., 1999 (remaining deposits); [2] M-miarolitic to pegmatitic quartz; V-vein quartz; P-quartz phenocryst; [3] coexisting melt inclusions present

[4] occurrence of ore minerals in the miarolitic cavities (e.g., Pezzotta et al., 1999).

(1) this study; (2) Audétat and Pettke, 2003; (3) Ulrich et al., 2002; (4) Redmond et al., 2004; (5) Landtwing et al., 2005; (6) Heinrich et al., 1999;
(7) Rusk et al., 2004; (8) Ulrich et al., 1999; (9) Williams-Jones and Heinrich, 2005; (11) Klemm et al., 2008; (12) Audétat et al., 1998;
(13) Audétat et al., 2000a; (14) Audétat et al., 2000b; (15) Zajacz et al., 2008; (16) Klemm et al., 2007

Samples were collected in a profile over ~100 m vertical distance in the northernmost part of the granite, from the bottom of the Carlink Canyon to the contact with the overlying country rocks. Additionally, two rhyolite dikes were sampled near the easternmost margin of the granite. Along the vertical profile, the granite changed in texture from

coarse-grained to porphyritic to aplitic. Miarolitic cavities up to 30 cm in diameter were found in the porphyritic and aplitic varieties within ~50 m of the upper contact. The mineralogy of these cavities is simple, comprising only quartz and orthoclase in most cases. Fluid inclusions of secondary and pseudosecondary origin are abundant in all samples. However, a few quartz crystals additionally contain primary fluid and melt inclusions arranged along former crystal surfaces (Fig. 2).
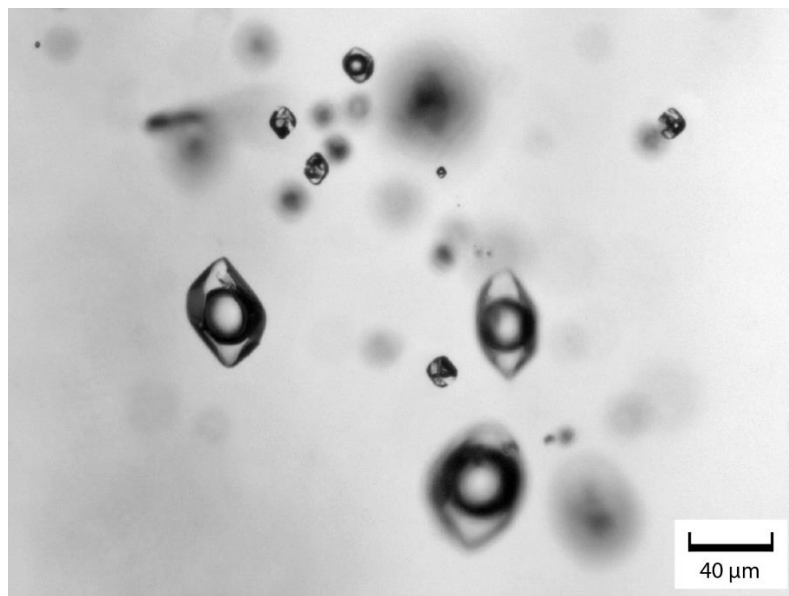

Figure 2. Large fluid inclusions and small, crystallized melt inclusions on a primary growth zone within a quartz crystal from a miarolitic cavity in the Stronghold Granite, Arizona. The fluid inclusions homogenize into the liquid phase at 396 to 421 °C, suggesting that the magmatic fluid was trapped in the single state field. Photomicrograph taken in transmitted light.

Aqueous fluid inclusions associated with melt inclusions were trapped in the single-phase field, are of medium density (degree of fill $F = vol_{liq}/vol_{tot} = 0.6$-$0.7$) and of low salinity (3.1-6.2 wt% $NaCl_{equiv}$), and homogenize near the critical point to the liquid phase at 396 to 421 °C. Younger fluid inclusions on pseudosecondary trails are either of lower salinity (0.9-4.2 wt% $NaCl_{equiv}$) and lower density ($F \leq 0.4$), or higher salinity (26-32 wt% $NaCl_{equiv}$) and higher density ($F \geq 0.8$). In some examples, both types of inclusions occur on the same trail (Fig. 3), demonstrating that they formed from a two-phase fluid (i.e., boiling assemblages). Trapping conditions of the fluid inclusions coexisting with melt inclusions were estimated from the intersection of the corresponding fluid isochores with the H_2O-saturated solidus curve of granites (e.g., Audétat and Pettke, 2003). Fluid isochores from two different miarolitic cavities in the Stronghold Granite intersect the solidus at 1.5 to 1.8 kbar and 670 to 700 °C (Fig. 4). Subsequent boiling assemblages were trapped at 420 to 510 °C and 250 to 600 bar. However, pressure estimates for the latter assemblages are associated with a large uncertainty because they are based on phase relations in the H_2O-NaCl model system, which may deviate from those in the analyzed fluid inclusions. Clathrates or liquid CO_2 were not observed in any of the fluid inclusions studied from the Stronghold granite.

Fluid/melt partition coefficients calculated from two pairs of coexisting melt and fluid inclusions were not constant (Fig. 5; Appendix 1). The partition coefficients of Pb, Zn, Mn and Cs, for example, are 2-3 times higher in the assemblage with the higher salinity fluid, probably reflecting the tendency of these elements to form aqueous chloride complexes (e.g., Webster et al., 1989; Seward and Barnes, 1997; Zajacz et al., 2008). The partition coefficients of Mo and W, elements thought to form hydroxyl complexes (e.g., Candela and Holland, 1984; Keppler and Wyllie, 1991; Candela and Piccoli, 1995) are significantly lower in the assemblage with lower fluid salinity.
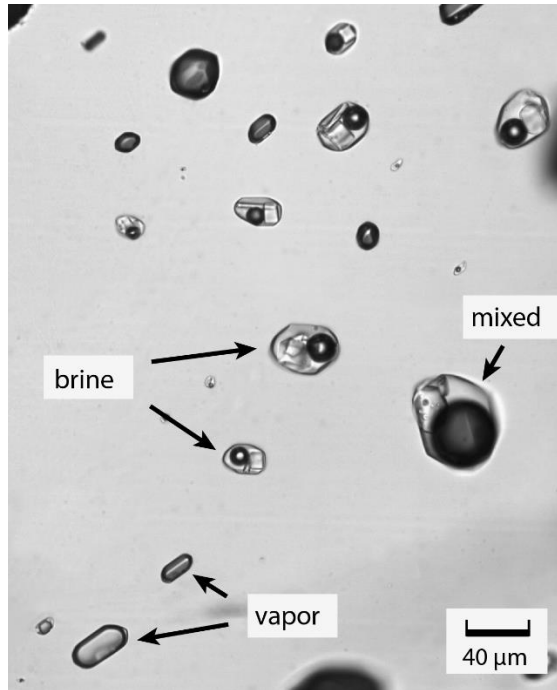
Figure 3. Vapor, brine and mixed vapor-plus-brine inclusions trapped along a single fracture plane within a quartz crystal from the Stronghold Granite, Arizona. The occurrence of two types of fluid inclusions with constant phase proportions suggests that the trapped fluid was in the two-phase field. The large inclusion on the lower right trapped an unknown proportion of both vapor and brine. The brine inclusions have a salinity of 46 wt% $NaCl_{equiv}$ and homogenize by bubble disappearance at 430 °C. Photomicrograph taken in transmitted light.
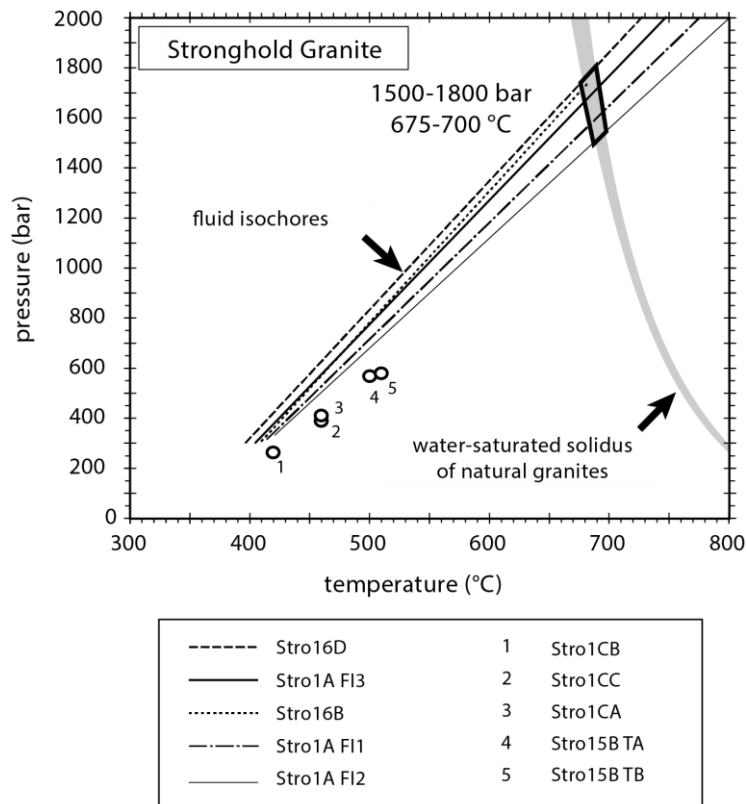

Figure 4. Reconstructed entrapment conditions of fluid inclusion assemblages in miarolitic quartz from the Stronghold Granite. Because these quartz crystals formed very late in the crystallization history of the pluton, the entrapment conditions of intermediate density fluid inclusions associated with melt inclusions can be estimated from the intersection of their corresponding isochores with the water-saturated solidus curve of granites. The entrapment conditions of subsolidus boiling assemblages (with pressure being estimated from phase relationships in the H_2O-NaCl model system) are shown by the open circles.
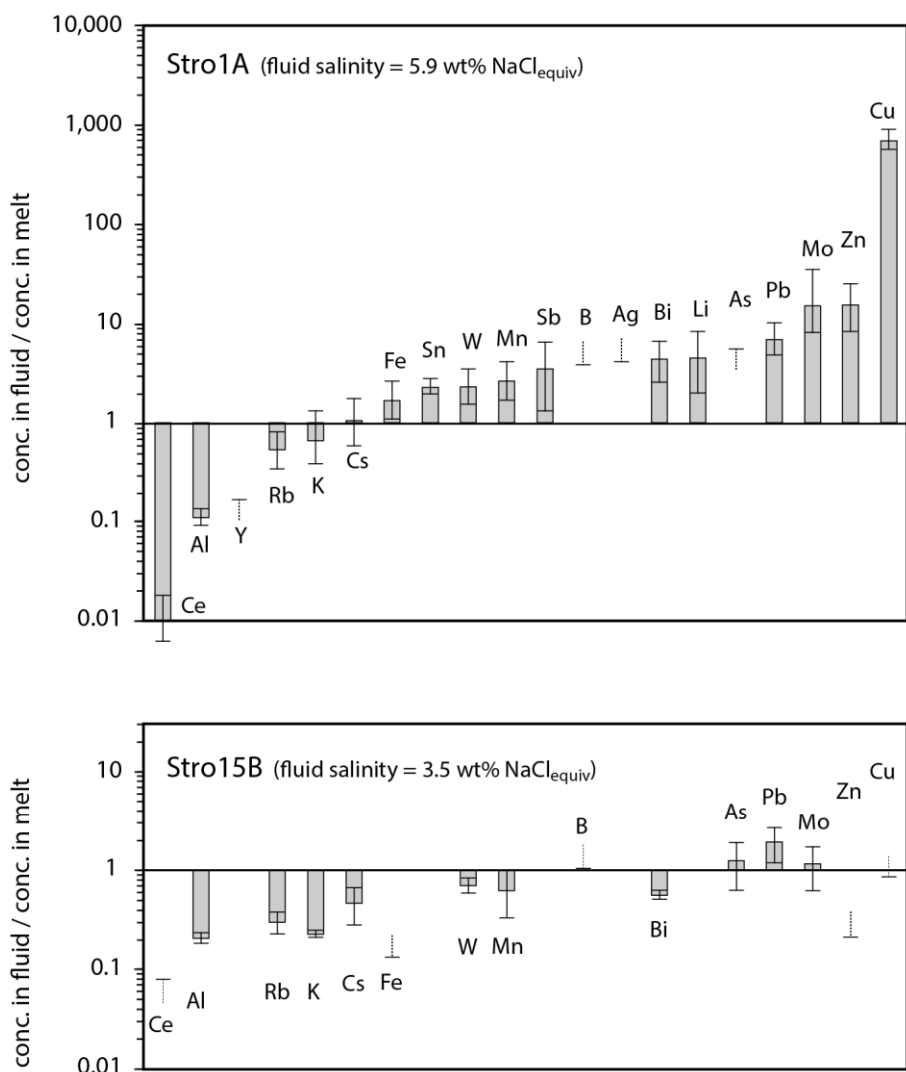
8

Figure 5. Fluid/melt partition coefficients calculated for two assemblages of coexisting fluid and melt inclusions in miarolitic quartz from the Stronghold Granite. In cases where elemental concentrations in the fluid or in the melt are below the detection limit, corresponding minimum or maximum partition coefficients are indicated by dotted error bars. Note that most partition coefficients are lower in the assemblage with the less saline fluid. Error bars represent maximum uncertainties that were calculated as follows: the upper points correspond to (avgfluid + stdevfluid)/(avgmelt - stdevmelt), whereas the lower points correspond to (avgfluid - stdevfluid)/(avgmelt + stdevmelt).

Cs concentrations in the fluid inclusions correlate positively with the Cs concentrations in the coexisting melt inclusions (Appendix 1; Cs content of the melt increases from 140 to 7600 ppm, and the Cs content of the fluid increases from 100 to 3600 ppm) but negatively with the fluid salinity (Fig. 6a), suggesting that the fluid salinity decreased with increasing degree of crystallization. This behavior is exactly as predicted by numerical models of granite crystallization at pressures > 1.3 kbar (Cline and Bodnar, 1991). The concentrations of Cu, Pb and Zn in the fluid decreased simultaneously with the fluid salinity, whereas W and Mo concentrations remained approximately constant (Fig. 6a). During the same fractionation interval the concentrations of W and Mo in the melt increased, whereas those of Pb and Cu remained constant or even decreased (Fig. 6b). The contrasting compositional trends observed in fluid versus melt inclusions require that the fluid/melt partition coefficients changed during fractional crystallization, as suggested by Figure 5. For example, the increase in the concentrations of W and Mo in the melt by about a factor of 5, but approximately constant concentrations of these elements in the coexisting fluid, agrees relatively well with the observed decrease in the fluid/melt partition coefficients of W and Mo by a factor of 4 and 12, respectively. Notice that the

increase of W and Mo in the residual melt does not contradict the fact that the measured fluid/melt partition coefficients are greater than unity, because at a pressure of 1.5 to 1.8 kbar (corresponding to a water solubility of 5-6 wt% H_2O in the melt), fluid/melt partition coefficients have to be greater than 17 to 20 to result in a net depletion of the corresponding elements in the melt.
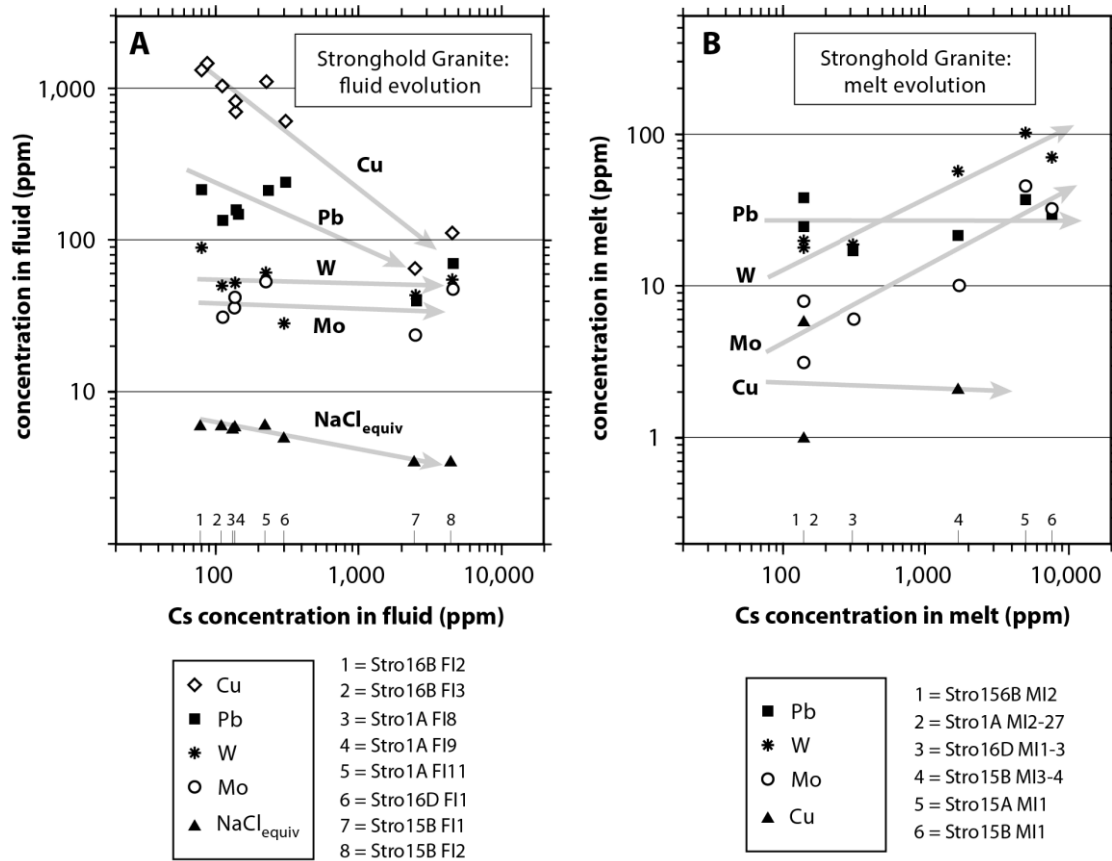

Figure 6. Compositional evolution of the magmatic fluid in the Stronghold Granite as a function of magma crystallinity, as recorded by increasing concentrations of Cs in the melt and in the fluid. The decrease in fluid salinity with increasing degree of melt fractionation agrees with numerical models of magma crystallization at > 1.3 kbar pressure. Small numbers and corresponding names refer to sample names used in the text, in Tables 2 and 3, and in Appendix 1.

3.2. Santa Rita: Large Cu (Mo-Au) porphyry ore deposit

The porphyry Cu deposit at Santa Rita, New Mexico (Chino Mine) is located in the Paleocene Santa Rita stock, which itself is part of a larger magma system that includes the skarn-mineralized Hannover-Fierro pluton to the north. Together, this area is referred to as the Central Mining district. An excellent summary of the geology of the district can be found in Rose and Baltosser (1966), and detailed geological and petrographic information is given by Jones et al. (1967). Important insights into the fluid evolution of Santa Rita were provided by Reynolds and Beane (1985), and two recent studies on the magmatic evolution of this magmatic-hydrothermal system were performed by Audétat et al. (2004) and Audétat and Pettke (2006). Mutschler et al. (1999) estimated the total production plus reserves for the Central Mining district at 8.7 Mt Cu, 1.3 Mt Zn, 160,000 t Pb, >80,000 t Mo, >16t Au, and 0.4 t Ag, close to the upper size limit of a large Cu deposit listed in the mining section of GIS Central Europe (http://giseurope.brgm.fr/). The Santa Rita mine currently produces Cu and Mo at a weight ratio of about 200 : 1 (Phelps Dodge Inc., 2006, Annual Report, Form 10-K, filed February 27, 2007, 359 p.). During a visit to the Santa Rita mine in 2000 a small miarolitic cavity in a boulder at the base of the North Pit was sampled. Although the exact origin of this boulder is unclear, it certainly originated from

within the North Pit. The miarolitic cavity is hosted by a 20 cm-wide aplite dike that cuts through quartz monzodiorite. Compared to the quartz monzodiorite the aplite is relatively unaltered, with no white mica alteration visible. Despite the relatively fresh appearance of the aplite dike, it appears to be related to mineralization, as molybdenite and chalcopyrite occur within the miarolitic cavity (Fig. 7a). This observation is in agreement with the finding of Rose and Baltosser (1966), who noted that in the Northern Pit, veins of magnetite and orthoclase are cut by veins or thin aplite dikes containing quartz, orthoclase, calcite and chalcopyrite. We therefore infer that the aplite dike formed in a late, synmineralization stage.
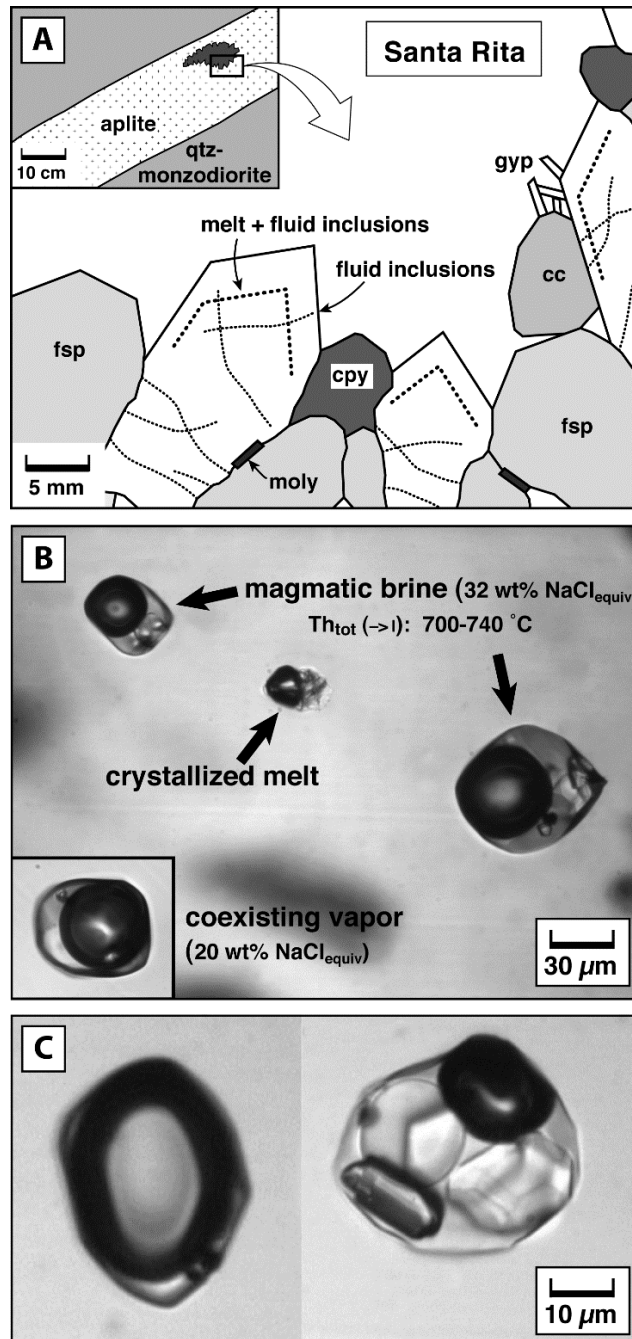
Figure 7. A. Schematic drawing of the spatial relationship between minerals, fluid inclusions and melt inclusions in a miarolitic cavity from Santa Rita, New Mexico (fsp = feldspar, moly = molybdenite, cpy = chalcopyrite, cc = calcite, gyp = gypsum). **B.** Photomicrograph of high-temperature (700-740 °C) vapor and brine inclusions associated with crystallized melt inclusions on a primary growth zone within miarolitic quartz. **C.** Photomicrograph of a vapor inclusion (left, 3 wt% NaCl$_{equiv}$) and a brine inclusion (right, 50 wt% NaCl$_{equiv}$) from a subsolidus boiling assemblage trapped at 460 °C (StaRita-6C).

11

Quartz crystals from the miarolitic cavity contain crystallized melt inclusions occurring in growth zones, as well as fluid inclusions ranging from contemporaneous with the melt inclusions to late secondary. Two types of fluid inclusions are closely associated with the melt inclusions (Fig. 7b): (i) one type that has a salinity of 33 wt% $NaCl_{equiv}$, a degree of fill of F ~ 0.6 and contains a small halite daughter crystal, and (ii) another type that has a salinity of 20-21 wt% $NaCl_{equiv}$ (i.e., halite-undersaturated at room temperature) and has a degree of fill of F~ 0.5. Inclusions of the more saline type homogenize into the liquid phase at 700 to 740 °C, whereas inclusions of the less saline type homogenize at the same temperature into the vapor phase. These characteristics are consistent with fluid entrapment at ~720 °C and 1250 bar in the two-phase field of the H_2O-NaCl system (Fig. 8a). These conditions plot on or slightly above the H_2O-saturated solidus curve of granite (Fig. 8b). Taken together, these observations strongly suggest that the two aqueous fluid phases exsolved directly from the crystallizing magma, which is in accord with the finding of Reynolds and Beane (1985).
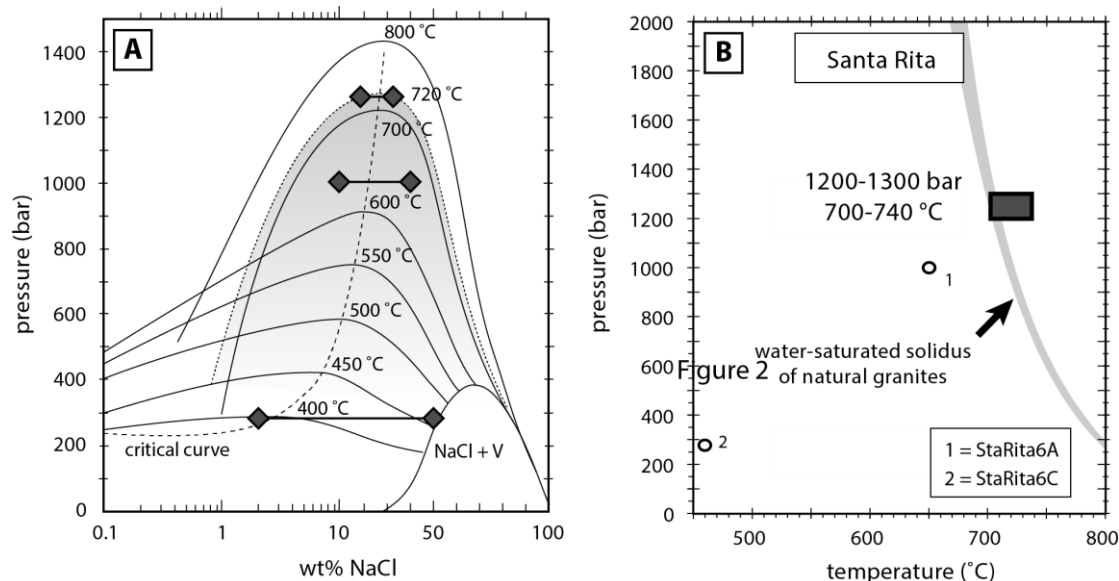

Figure 8. A. P-X diagram of the system H_2O-NaCl, showing the estimated entrapment conditions of three boiling assemblages analyzed from Santa Rita. Entrapment pressures were estimated by intersecting the salinity of brine inclusions with the isotherms corresponding to their homogenization temperature. **B.** P-T plot showing the entrapment conditions derived in (A) in relation to the water-saturated solidus of natural granites (Luth et al., 1964; Piwinskii and Wyllie, 1970; Jahns, 1982). The fact that the P-T conditions estimated for the highest temperature vapor and brine inclusions overlaps with the granite solidus confirms that they were trapped at magmatic conditions, as also implied by their coexistence with melt inclusions.

Slightly younger (but still >600 °C) boiling assemblages contain 31 wt% $NaCl_{equiv}$ brine inclusions that coexist with 10 wt% $NaCl_{equiv}$ vapor inclusions; another boiling assemblage that formed at 460 °C contains 50 wt% $NaCl_{equiv}$ brine inclusions that coexist with 3 wt% $NaCl_{equiv}$ vapor inclusions (Fig. 7c). As the temperature and pressure decrease, the observed salinity of the vapor phase deviates significantly from that predicted for the experimentally determined H_2O-NaCl system, a phenomenon that is observed in nearly all natural samples. The two most likely explanations for this behavior are: (i) at lower pressures and temperatures the phase relations in the real system deviate significantly from those in the simple H_2O-NaCl system because of the presence of other components, or (ii) the vapor-rich inclusions have been affected by trapping small amounts of liquid along with the vapor. In the latter scenario, the higher temperature inclusions would not be greatly affected (trapping a portion of 33 wt% liquid along with the 22 wt% vapor will not significantly change the salinity of the vapor inclusion), but trapping even a small amount of 50 wt percent liquid along with the 3 wt percent vapor at 460°C will have a large effect on the salinity of the vapor-rich inclusions, as found by Bodnar et al. (1985) in their experimental study. Vapor-brine partition coefficients for the three highest-

temperature boiling assemblages analyzed from Santa Rita (650-720 °C) are shown in Figure 9, and absolute metal concentrations are shown in Figure 10. With increasing Cs concentration in the fluid (whether in brine or vapor) the Cu content decreased, whereas Mo and W concentrations increased, and Pb concentrations as well as fluid salinities stayed approximately constant. The lack of a significant change in fluid salinity is in accord with fluid entrapment at magmatic conditions, because in the system melt + two fluid phases the concentration of chlorine in all three phases is fixed (e.g., Shinohara, 1994).
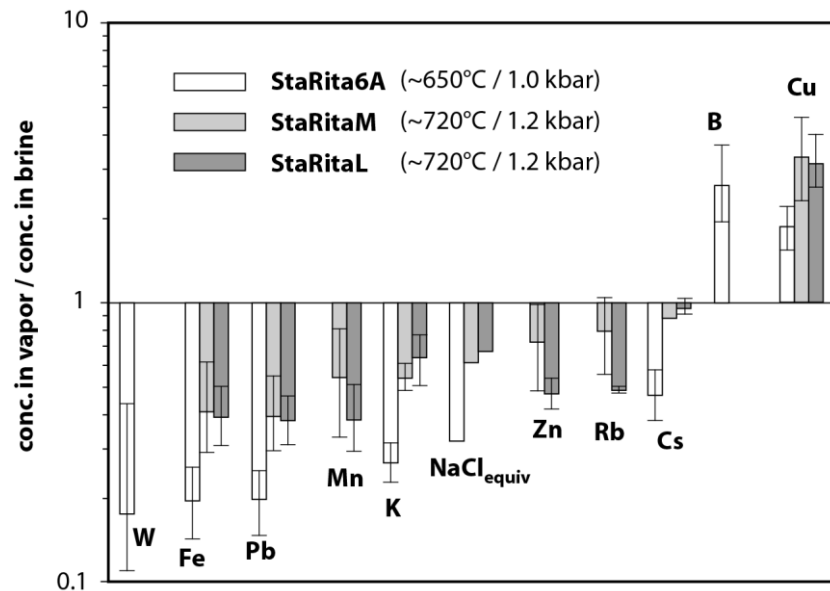
Figure 9. Vapor/brine partition coefficients determined on three different boiling assemblages in miarolitic quartz from Santa Rita, New Mexico. See caption of Fig. 5 for the definition of the error bars.
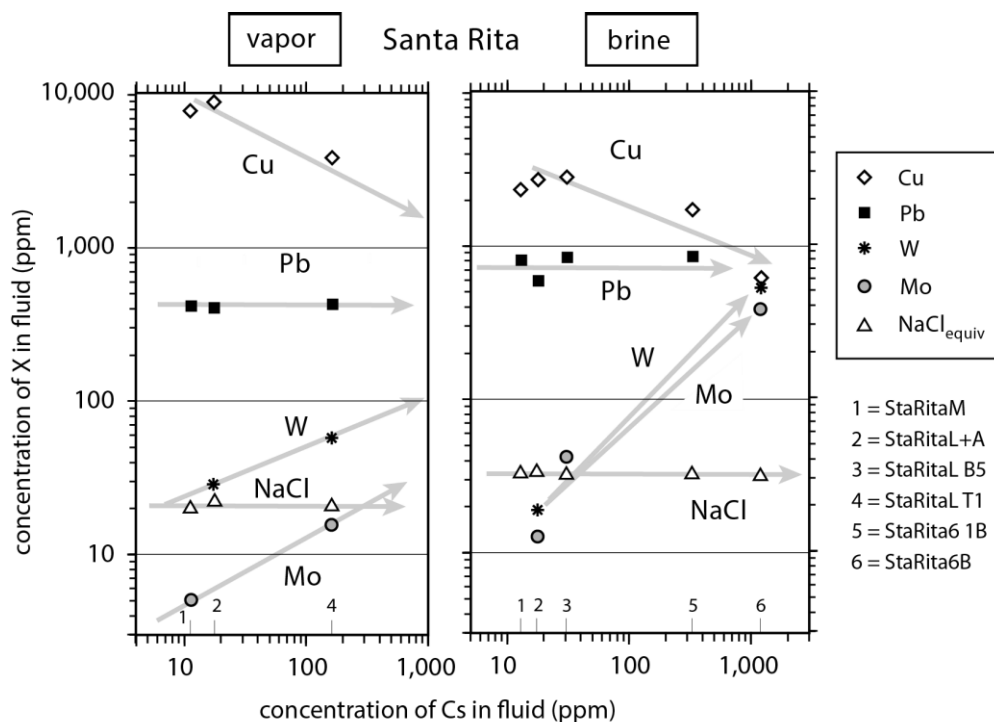
Figure 10. Compositional evolution of magmatic vapor and brine trapped in miarolitic quartz at Santa Rita, New Mexico, plotted as a function of increasing Cs concentration in the fluid. Note that in both vapor and brine the concentrations of Mo and W increase with increasing degree of melt fractionation, whereas those of Cu and Pb either decrease or remain constant. The salinities of vapor and brine remain constant during melt evolution at constant temperature and pressure because in the system melt + vapor + brine the chlorine content of each phase is fixed (but the relative proportions of the phases can vary).

3.3. Cave Peak: Large Mo-Nb (Cu-W) porphyry ore deposit

The 32-39 Ma old Cave Peak prospect in northwestern Texas hosts three distinct molybdenum orebodies centered on a porphyry plug within a breccia pipe (Sharp, 1979). Several intrusive phases were distinguished based on surface mapping and extensive drilling. The first intrusive event is represented by a quartz latite to quartz monzonite porphyry, followed by eruption of rhyodacite and concomitant development of a breccia pipe with a rhyolitic groundmass. The breccia pipe and the quartz monzonite porphyry were then intruded by a second quartz monzonite porphyry (phase II) and late rhyolite porphyry dikes. Crosscutting relationships demonstrate that the quartz monzonite porphyry of phase II is younger than the formation of the uppermost Mo orebody, but earlier than the formation of the two lower orebodies (Sharp, 1979). The deposit, which has not yet gone into production, hosts a resource of 200 to 500 Mt ore averaging 0.2-0.3 wt% Mo and 0.1 wt% Nb_2O, of which at least 30 Mt contain also 0.05 wt% Cu and 0.01 wt% W (Long, 1992; Mutschler et al., 1999).
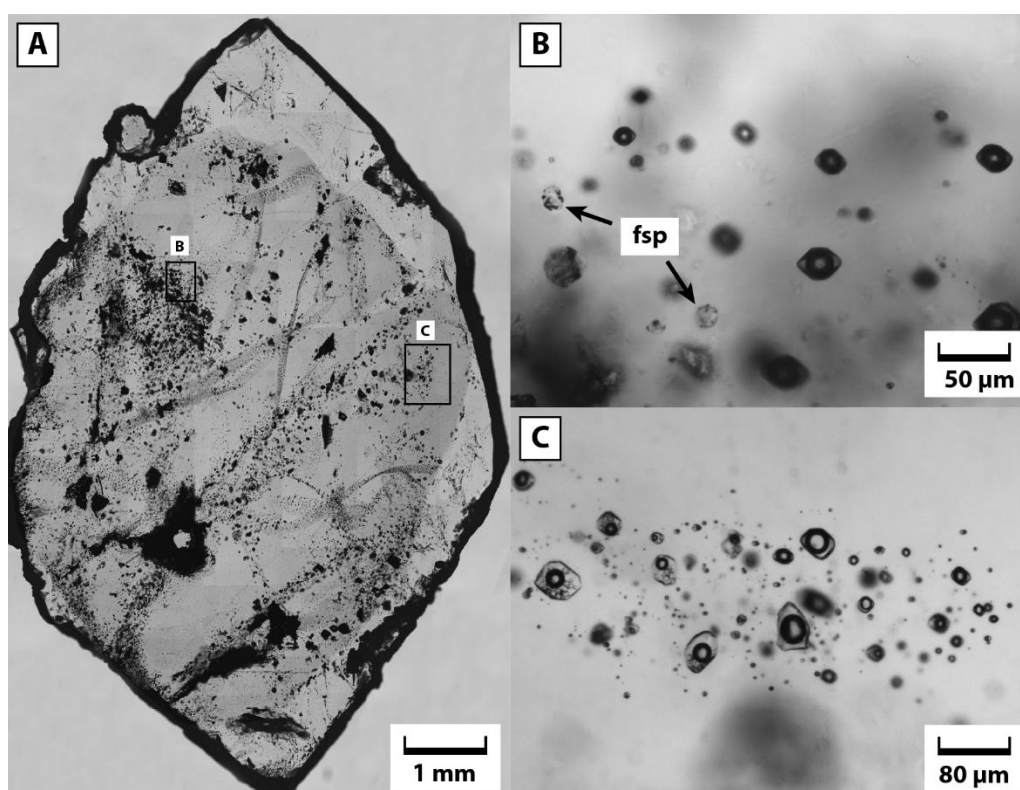

Figure 11. Fluid inclusions in a quartz crystal from the Mo-Nb porphyry at Cave Peak, Texas. **A.** Doubly polished thick section along the c-axis of the crystal, showing a smoky colored core and a colorless overgrowth. At the border between the two quartz generations small inclusions of molybdenite, columbite, biotite, cassiterite and yttrofluorite are present. **B.** Enlargement of the fluid inclusion cluster in the upper left of the crystal, showing high-temperature vapor inclusions (3.1 wt% NaClequiv; Thom = 600 °C) next to feldspar inclusions (fsp). **C.** Enlargement of a primary, pre-mineralization fluid inclusion cluster in the right part of the crystal, containing brine inclusions (38.2 wt% NaClequiv; Thom = 530-540 °C) and coexisting vapor inclusions (4.0 wt% NaClequiv).

Samples were collected from druses and veins within the rhyolitic groundmass of breccia cropping out south of the exposed phase II quartz monzonite porphyry. A drusy quartz vein within a strongly silicified igneous rock fragment contains smoky quartz crystals up to 10 mm in length that grew into open spaces and are covered by small fluorite octahedra as well as iron oxides. A cross section through one of these crystals (sample CP1) is shown in Figure 11a. Two stages of crystal growth are apparent: (i) an early stage of smoky quartz and (ii) a later stage of colorless quartz. Along the contact between the two stages, numerous inclusions of molybdenite, biotite, columbite, cassiterite and yttrofluorite are

present. Many pseudosecondary fluid inclusion trails in the smoky quartz end at this contact (e.g., CP1A trail A, CP1D-A and CP1D-C; Appendix 1). Accordingly, fluid inclusions on these pseudosecondary trails are classified as pre- to synmineralization. Other fluid inclusions occur within clusters that are entirely hosted by smoky quartz and, thus, can be classified as pre-Mo mineralization (Fig. 11b, c). Both vapor and brine inclusions are present in these clusters, with vapor inclusions being dominant in the clusters in the center of the crystal, and about equal numbers of vapor and brine inclusions occurring in the clusters near the contact with colorless quartz. Vapor inclusions in the large cluster on the upper left (CP1AA core; Fig. 11b) have a degree of fill of F ~ 0.5 and a salinity of 3.1 wt% $NaCl_{equiv}$, whereas rare, coexisting brine inclusions have a degree of fill of F ~ 0.85 and a salinity of 38.2 wt% $NaCl_{equiv}$. Both types of inclusions attain total homogenization at about 600 °C. A high-temperature origin for these fluid inclusions is supported by the composition of coexisting feldspar inclusions (Fig. 11b), which range from $Ab_{34}Or_{66}$ to $Ab_{40}Or_{60}$ (determined by LA-ICP-MS by drilling out entire inclusions). Due to the presence of a solvus in the system albite-orthoclase, intermediate feldspars of this composition can only exist at ≥610-640 °C (Tuttle and Bowen, 1958). A cluster of brine and vapor inclusions (38.2 wt% $NaCl_{equiv}$ and 4.0 wt% $NaCl_{equiv}$, respectively) closer to the contact with colorless quartz (but still fully within smoky quartz) hosts similar fluid inclusions but no feldspar inclusions (CP1AA prib; Fig. 11c). Brine inclusions in this cluster homogenize at 530-540 °C. Sample CP5 is a 5 mm-long quartz crystal collected from a different vein, hosting a secondary trail with 6.2 wt% $NaCl_{equiv}$ vapor inclusions coexisting with 47.4 wt% $NaCl_{equiv}$ brine inclusions , the latter homogenizing at 450 °C.
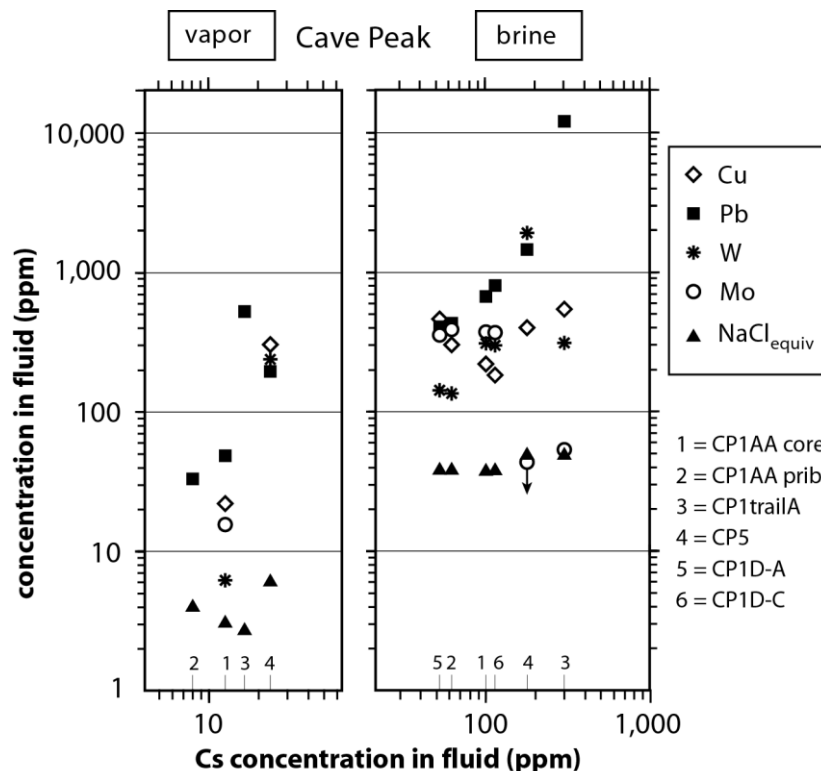
Figure 12. Relationship between Cs concentration, fluid salinity and metal content of medium to high-temperature (450-600 °C) vapor and brine inclusions from Cave Peak. Pseudosecondary trail "CP1trailA" starts at the boundary between smoky quartz and colorless quartz in Fig. 11a and thus formed at the same time as Mo-W-Nb-Ta mineralization. This explains the relatively low concentrations of W and Mo in the brine on this trail relative to that in earlier, higher temperature brines analyzed in this sample.

LA-ICP-MS analyses of vapor inclusions in the primary clusters in CP1AA indicate Mo concentrations of 16 ± 4 ppm and Cu concentrations of 22 ± 11 ppm. The latter are extremely low compared to vapor inclusions found in porphyry Cu deposits (e.g.,

15

Williams-Jones and Heinrich, 2005). Coexisting brine inclusions, on the other hand, contain 370 to 390 ppm Mo and 180 to 300 ppm Cu, plus 60 to 100 ppm Nb, 130 to 290 ppm W and 430 to 790 ppm Pb (Appendix 1, Fig. 12). In both vapor and brine inclusions, the concentrations of Pb and W increase with increasing Cs content, whereas for Cu and Mo no trends are apparent. Note that in all three measured boiling assemblages Cu partitioned preferentially into the brine phase, in contrast to the behavior observed in porphyry Cu and many other types of ore deposits (e.g., Heinrich et al., 1999; Williams-Jones and Heinrich, 2005). Molybdenum concentrations in the brine are 360 to 410 ppm in the two synmineralization trails CP1D-A and CP1D-C, but only 54 ppm and <45 ppm in the syn-mineralization trail CP1AA-trail A and in sample CP5, respectively (Fig. 12). The fact that the concentration of Mo decreased while that of other metals such as Cu and Pb remained constant or even increased suggests that molybdenum precipitated during this stage; this is consistent with the presence of molybdenite (but absence of Cu and Pb-bearing minerals) along the contact between the two quartz generations.

3.4.   Barren Rito del Medio pluton

The fluid and melt evolution of the barren Rito del Medio pluton in northern New Mexico is described in detail in Audétat and Pettke (2003). Here we summarize only the information relevant for this comparative study. The Rito del Medio pluton is one of four resurgent plutons that intruded the Questa caldera soon after its collapse at 25.7 Ma. It is a metaluminous granite composed of alkali feldspar (57-66 vol%), quartz (29-38 vol%), plagioclase (<1 vol%), biotite (0.5-1.6 vol%) and muscovite (0-1 vol%), with SiO_2 contents ranging from 76 to 78 wt percent (Johnson et al., 1989). No mineralization is known at the present level of exposure.
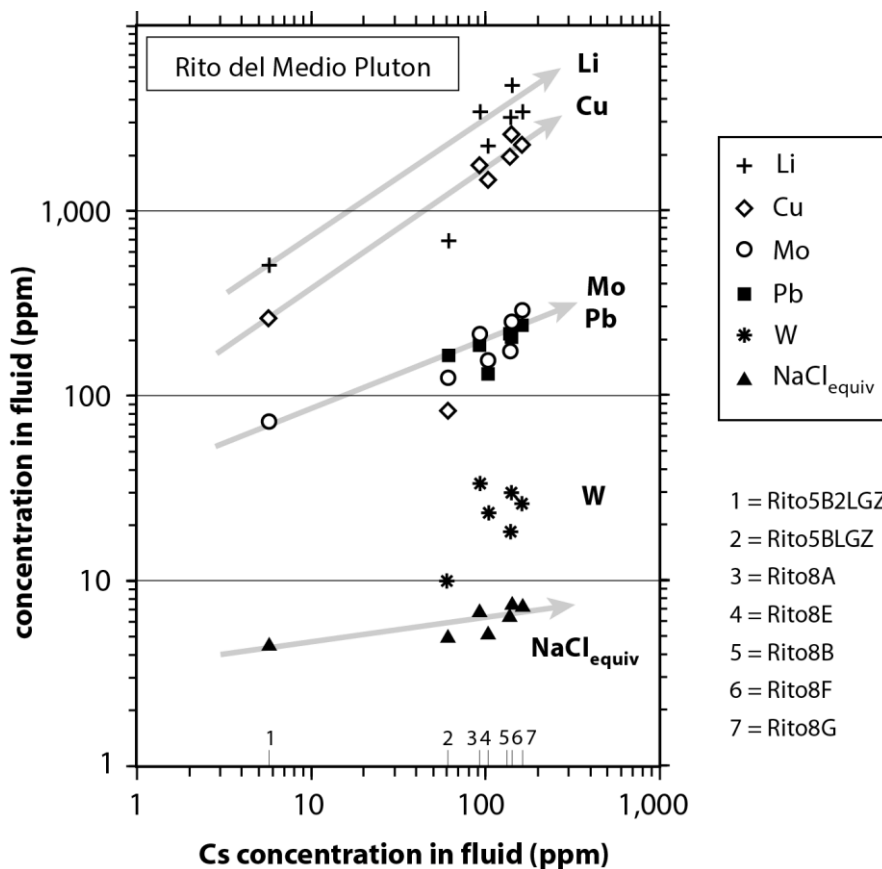

Figure 13. Compositional evolution of the magmatic, single-phase fluid in the Rito del Medio Pluton, New Mexico, as a function of melt fractionation. The increase in fluid salinity with increasing degree of melt fractionation is in agreement with numerical models of magma crystallization at <1.3 kbar pressure.

16

Coexisting fluid and melt inclusions in quartz crystals from miarolitic cavities demonstrate that a single-phase, low-salinity (4.5-7.5 wt% NaCl$_{equiv}$), low-density (F= 0.4-0.3) aqueous fluid exsolved from the crystallizing melt at 1.1 to 1.3 kbar and 700 to 720 °C. This single-phase fluid subsequently split into coexisting vapor (1.2-3.7 wt% NaCl$_{equiv}$) and brine (26.0-29.6 wt% NaCl$_{equiv}$) at lower pressure and temperature (Audétat and Pettke, 2003). The compositional evolution of the single-phase fluid is shown in Figure 13. With increasing Cs content of the fluid both the salinity and the metal content increased, reaching more than 2000 ppm Cu and 200 ppm each of Mo and Pb in the most fractionated fluids. Brine inclusions in the subsolidus boiling assemblages contain 530 to 1600 ppm Cu, 20 to 760 ppm Mo, 20 to 90 ppm W and 1300 to 2100 ppm Pb (Appendix 1). The increase in the salinity of the single-phase fluid with increasing melt fractionation (as monitored by rising Cs concentrations) is consistent with the fluid evolution predicted for magmas crystallizing at ≤ 1.3 kbar (Cline and Bodnar, 1991).

3.5. Mole Granite: Large Sn-W (Cu-Ag-Pb-Zn) ore deposit

The 248 Ma Mole Granite in eastern Australia is associated with more than 1200 small ore deposits that were mined primarily for Sn and W and to a smaller degree for Cu, As, Bi, Au, Pb, Zn and Ag (Henley et al., 1999, 2000). The intrusion is exposed over an area of about 30x50 km and is geochemically rather homogeneous despite the existence of three distinct textural variants. The ore deposits are arranged in well-defined metal zones, with Sn deposits occurring preferentially within the central body of coarse-grained granite, W (-Bi, Au) deposits within the 10-100 m thick carapace of porphyritic granite, and base metal deposits within the overlying sedimentary rocks. Quartz crystals that grew into open spaces in veins within the granite have been studied in detail by Eadington (1983), Sun and Eadington (1987), Audétat et al. (1998, 2000b), and Audétat and Günther (1999). Using the chemical evolution of brine inclusions and oxygen isotopic data (Sun and Eadington, 1987), it has been demonstrated that Sn and W ore precipitation was triggered by mixing between magma-derived fluids (400-600 °C) and invading meteoric water (350-400 °C). Numerous boiling assemblages document that at temperatures between 400 and 600 °C the fluid was mostly in the two-phase field. Below 350 to 400°C, fluid inclusions were generally trapped in the single-phase field.

Aqueous fluid inclusions associated with melt inclusions occur in igneous topaz crystals and in former embayments within quartz phenocrysts (Audétat et al, 2000a). These magmatic fluid inclusions are vapor-rich, with F ~ 0.2-0.3 and a salinity of 4.5 to 8.0 wt% NaCl$_{equiv}$. Most of them are small (≤ 20 µm); therefore, only a few could be analyzed by LA-ICP-MS. Large, well-preserved fluid inclusions trapped at magmatic or near-magmatic temperatures have recently been found in a quartz crystal from the same miarolitic cavity as sample Leno1 described by Audétat et al. (2000b). Clusters of randomly distributed, low-density (F ~ 0.2-0.3), low-salinity (3.1-4.5 wt% NaCl$_{equiv}$) fluid inclusions in the central part of this crystal (Leno2; Fig. 14) are intersected by well-defined trails of high-temperature boiling assemblages. This textural relationship suggests that the vapor inclusions in the clusters were trapped earlier, and thus probably at higher temperatures than the boiling assemblages. Trail D, which is the oldest pseudosecondary trail identified in this sample, contains brine inclusions that homogenize at 620 °C, whereas those on trail H homogenize at 580 °C. The vapor fluid inclusions in the older clusters, on the other hand, homogenize at 420 ±10 °C (homogenization temperatures could be well determined in five inclusions with flat, pointy tips). The markedly lower homogenization temperatures of these early vapor fluid inclusions in comparison with that of later brine inclusions suggests that the former were trapped in the single-phase field. Corresponding fluid isochores intersect the granite solidus at 710 to 730 °C / 950 to 1000 bar, which agrees well with the final crystallization conditions inferred for the Mole Granite (Audétat

et al., 2000a). The compositions of the earliest fluid inclusions in Leno2 are compared with those of other single-phase fluid inclusions of the Mole Granite in Figure 15. With increasing Cs concentration in the fluid there was an increase in B, W and fluid salinity, whereas Cu strongly decreased and As, Pb, Bi and Sn remained more or less constant. The increase in fluid salinity with increasing melt crystallinity is consistent with crystallization of granitic magmas at pressures $\leq$ 1.3 kbar (Cline and Bodnar, 1991).
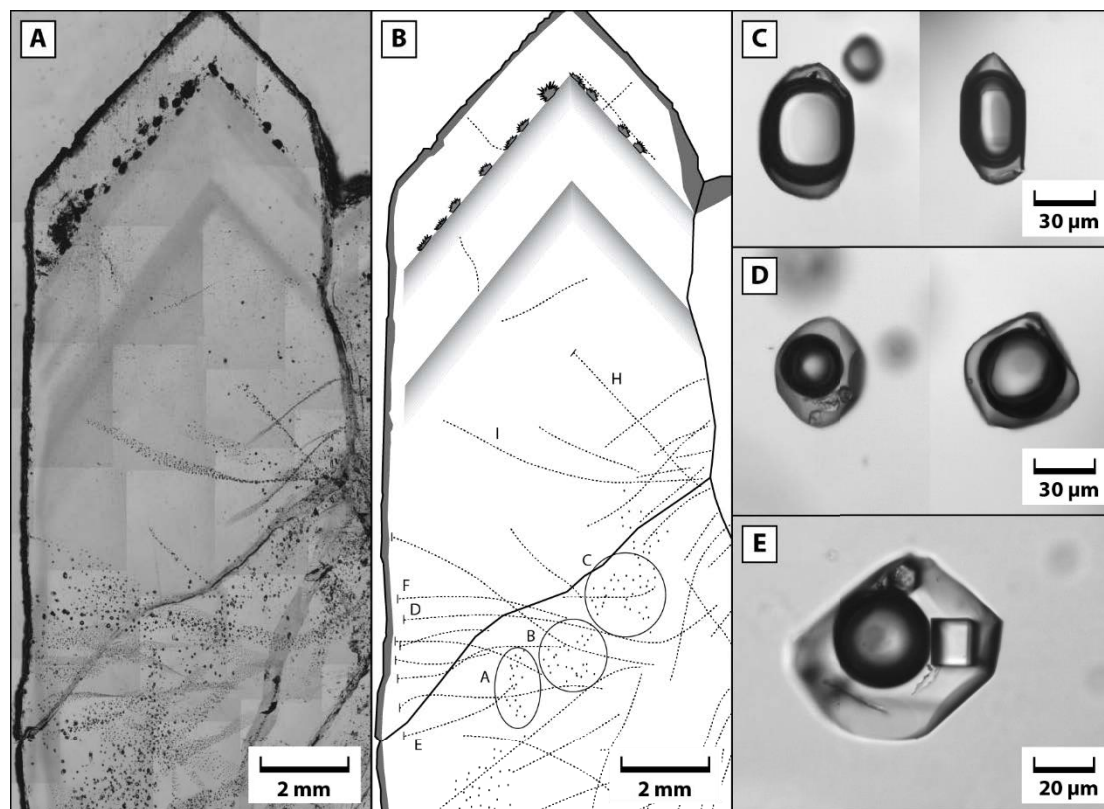

Figure 14. Petrographic relationships and optical appearance of fluid inclusions in quartz crystal "Leno2" from a miarolitic cavity in the Mole Granite, Australia. **A.** Doubly polished section through the c-axis of the crystal. **B.** Petrographic interpretation of the photograph shown in A. Notable are areas of randomly distributed fluid inclusions in the core of the crystal (e.g., areas marked as A, B and C), which contrast with fluid inclusions on well-defined trails (dotted lines). Some of these trails end abruptly at former crystal surfaces (marked by a T-bar at the end of the trail; e.g., upper end of trail H), identifying them as pseudosecondary. **C.** Two examples of fluid inclusions from the clusters in the core of the crystal. They are characterized by a low density (degree of fill 0.2-0.3) and a low salinity (3.1-4.5 wt% NaCl$_{equiv}$), and homogenize into the vapor phase at about 420 °C. **D.** Brine inclusion (left) and coexisting vapor inclusion (right) on pseudosecondary trail D. The brine inclusion has a salinity of 28.4 wt% NaCl$_{equiv}$ and homogenizes into the liquid phase at >600 °C. **E.** Brine inclusion on pseudosecondary trail F, which seems to be younger than trail D because it starts closer to the rim of the crystal. Brine inclusions on this trail have a salinity of 30.9 wt% NaCl$_{equiv}$ and homogenize into the liquid phase at 525 °C. All photographs taken in transmitted light.

3.6.   Capitan Mountains: Subeconomic Th-U-REE mineralization

The 28.3 ± 0.04 Ma Capitan pluton is one of the largest Tertiary intrusions in New Mexico. The compositionally and texturally zoned pluton was emplaced at a shallow depth ($\leq$ 2.3 km: Allen and McLemore, 1991) and is only partly unroofed. It is associated with three types of mineralization: (1) iron skarns and veins, (2) manganese veins, and (3) veins and breccias containing quartz, fluorite and locally high concentrations of U, Th, REE, Au and Ag (McLemore and Phillips, 1991). The composition and distribution of fluid inclusions in this pluton was studied extensively by Ratajeski and Campbell (1994), Campbell et al. (1995) and Campbell (1995). For the present study samples were collected from porous breccia zones in the uppermost, granophyric facies (i.e., the "bubble zones" of Campbell, 1995), as well as from the allanite-mineralized Mina Tiro Estrella (MTE) prospect in the

18

porphyritic granite facies. We also studied fluid inclusions in phenocrystic quartz of the granophyric variety, although it was noted that the inclusions show signs of post-entrapment water loss. In these latter samples both high-salinity brine inclusions (60-67 wt% $NaCl_{equiv}$; Th_{tot} = 630-690 °C) and low-density (F ≤ 0.1) vapor inclusions (ca. 2 wt% $NaCl_{equiv}$) coexist with melt inclusions, suggesting that these two types of fluid exsolved simultaneously from the melt (Fig. 16a). In contrast to this, only high-salinity brines (72.5 wt% $NaCl_{equiv}$; Th_{tot} = 595 °C) were trapped in quartz from the "bubble zones", and in vein quartz from the MTE prospect (Fig. 16b). These observations agree with the findings of Ratajeski and Campbell (1994), Campbell et al., (1995) and Campbell (1995).

Brine inclusions from the MTE prospect contain high concentrations of REE (300 ppm Ce, 270 ppm La) and U (17 ppm) but relatively low concentrations of Cs (70 ppm), Cu (70-600ppm), Pb (470 ppm), Mo (80 ppm), Sn (60 ppm), Bi (5 ppm) and W (30 ppm) (Appendix 1). Two brine inclusions associated with melt inclusions in quartz phenocrysts from the granophyric variety (which is the most fractionated rock type in the Capitan pluton: Allen and McLemore, 1991) display a more fractionated fluid composition, with higher concentrations of Cs (610 ppm), Mo (1100 ppm), Sn (180 ppm), W (460 ppm), Bi (30 ppm), Pb (5500 ppm) and Cu (790 ppm), but similar concentrations of REE (390 ppm Ce) and U (20 ppm). Three vapor inclusions (~ 2 wt% $NaCl_{equiv}$; salinity not well constrained due to poor visibility of phase transitions) from the same rock type reveal low concentrations of Cu (70-130 ppm) but relatively high concentrations of Ce (13 ppm) (Appendix 1).
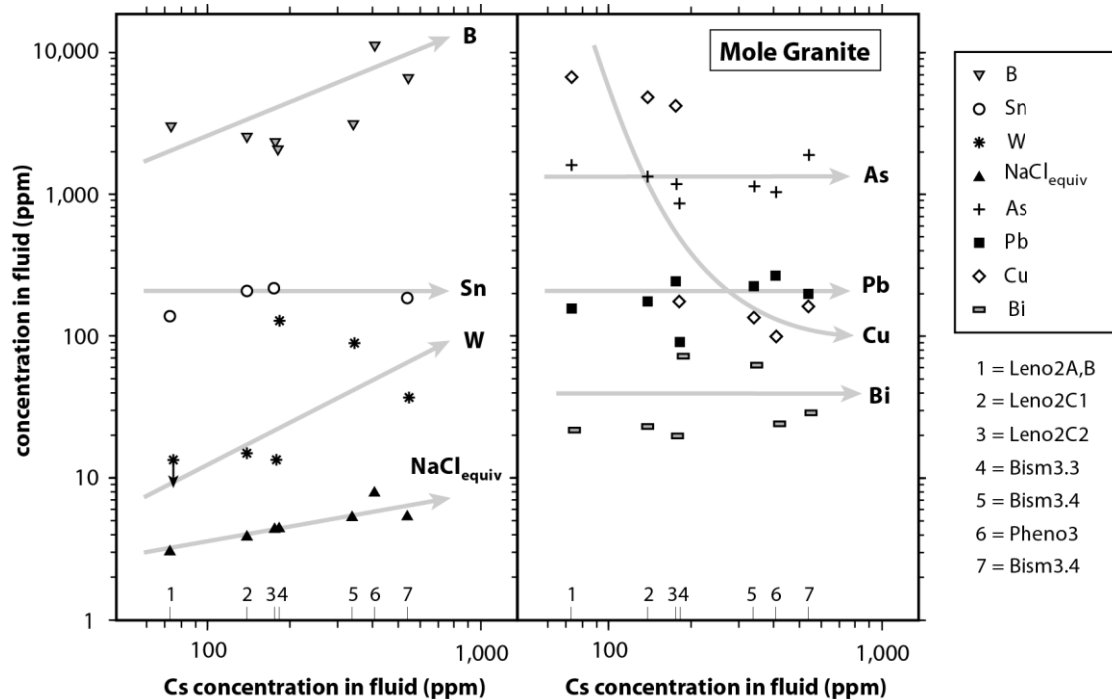

Figure 15. Compositional evolution of magmatic, single-phase fluids in the Mole Granite, Australia. The increase in fluid salinity with increasing degree of melt fractionation (as recorded by the Cs concentration in the fluid) is in agreement with numerical models for magma crystallization at <1.3 kbar.
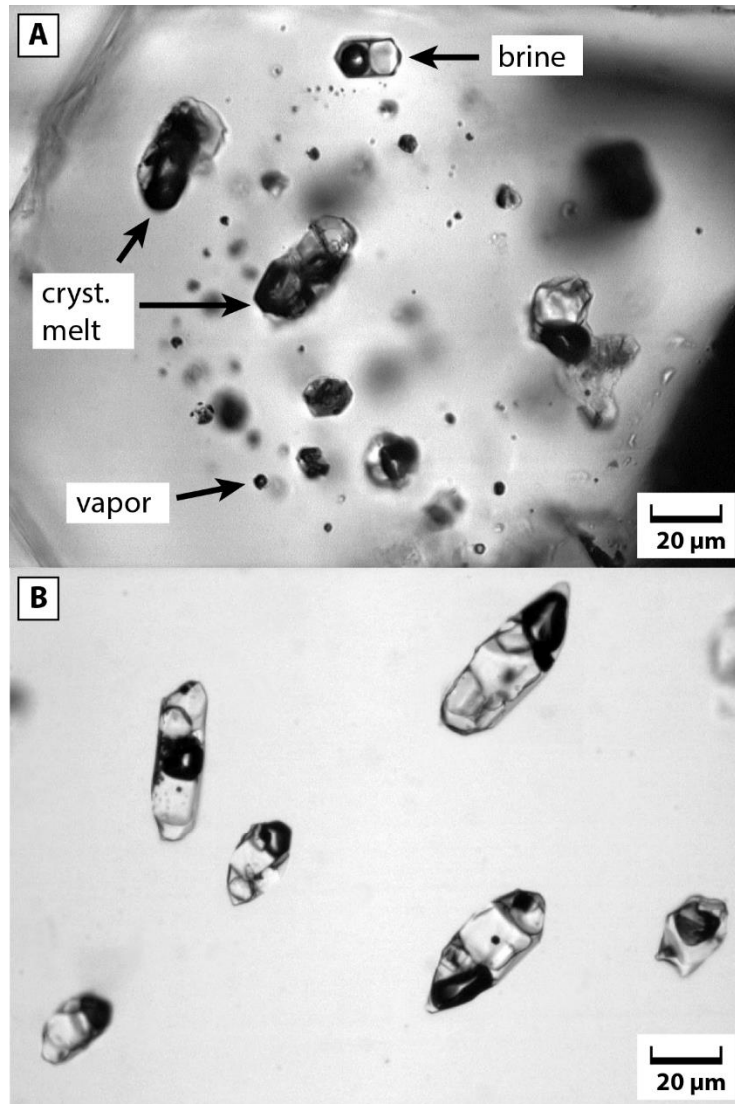
Figure 16. A. Crystallized melt inclusions coexisting with vapor inclusions (ca. 2 wt% NaCl$_{equiv}$) and brine inclusions (60-67 wt% NaCl$_{equiv}$; Th$_{tot}$ = 630-690 °C) in the core of a quartz phenocryst from the granophyric granite variety in the uppermost part of the Capitan Pluton, New Mexico. **B.** High-salinity (72 wt% NaCl$_{equiv}$), high-temperature (Th$_{tot}$ = 595 °C) brine inclusions in vein quartz from the REE-mineralized Mina Tiro Estrella prospect on the southern rim of the pluton.

3.7. Summary of fluid properties in barren and mineralized intrusions

Table 1 summarizes the physical and chemical properties of the earliest (i.e., highest temperature, 600-720 °C) fluid inclusions found in the six intrusions described above, and compares these characteristics with those of high-temperature fluids reported from eleven other occurrences (4 barren, 7 mineralized). In 10 out of the 17 localities listed in this table the earliest fluid found was single phase and of relatively low salinity (2-13 wt% NaCl$_{equiv}$; average 5 wt% NaCl$_{equiv}$) and low density (F ≤ 0.5). Such properties of an early magmatic fluid are in agreement with theoretical considerations (e.g., Burnham, 1967, 1979, 1997), with earlier studies on porphyry systems (e.g., Roedder, 1971; Roberts, 1975; Bodnar, 1982, Fluid inclusions in porphyry-type deposits: Mineral Deposits Research Review for Industry Course Notes, p. RB1-25; Shinohara and Hedenquist, 1997) and with estimates based on the composition of melt inclusions and magmatic apatite phenocrysts (Piccoli and Candela, 1994; Gerlach et al., 1996; Stix and Layne, 1996). However, depending on bulk fluid composition and confining pressure the first exsolved fluids can also be two phase (e.g., Bodnar et al., 1985; Webster, 1992; Shinohara, 1994;

Bodnar, 1995; Webster and Mandeville, 2007). Exsolution of two fluid phases from the melt is observed at Cuasso al Monte, Mt. Malosa, and the Capitan pluton (all barren), as well as Santa Rita (Table 1). Two types of high-density vapor inclusions are described from Bajo de la Alumbrera (Ulrich et al., 2002), of which one type potentially represents a single-phase parent fluid. At Grasberg and Cave Peak only subsolidus boiling assemblages were found (Table 1); therefore, we cannot tell whether the fluid that exsolved at magmatic conditions was single phase or two phase. The fact that at several localities no samples with fluid inclusions trapped in the one-phase field were found poses a problem, as a rigorous comparison with other occurrences can only be made if the composition of the *bulk* fluid (i.e., the mass ratio between vapor and brine) is known. A potential way to obtain this missing information is outlined below.

4. Calculation of the Composition of Parent Fluids Based on Two-phase Boiling Assemblages

At all localities in which fluid inclusions representative of early, single-phase fluids were found (i.e., the parental fluids prior to the intersection of their solvus), there are also subsequent generations of boiling assemblages present. We can assume that some of these boiling assemblages formed from a common single-phase fluid by phase separation, with separation occurring at two different pressure and temperature conditions (Fig. 17). In the example shown in Figure 17, a single-phase fluid with a salinity of 5 wt% NaCl at 700 °C and 1200 bar (S) separates to boiling assemblage A at 600 °C and 820 bar and to boiling assemblage B at 550 °C and 680 bar. As a result, vapor forms with the mass fractions x and y, respectively (solid, horizontal lines), and brine with the mass fractions (1-x) and (1-y), respectively (dashed, horizontal lines). If both phase separations occurred in a locally closed system from the same bulk composition (i.e., from the same parent fluid), we can establish a set of mass balance equations for any two elements occurring in the fluids (Cu and Na being chosen here for example):

$$Cu^{bulk} = x \cdot Cu_A^{vap} + (1-x) \cdot Cu_A^{brine} \tag{1}$$

$$Cu^{bulk} = y \cdot Cu_B^{vap} + (1-y) \cdot Cu_B^{brine} \tag{2}$$

$$Na^{bulk} = x \cdot Na_A^{vap} + (1-x) \cdot Na_A^{brine} \tag{3}$$

$$Na^{bulk} = y \cdot Na_B^{vap} + (1-y) \cdot Na_B^{brine} \tag{4}$$

Combining (1) with (2) gives:

$$x = \frac{y \cdot \left(Cu_B^{vap} - Cu_B^{brine}\right) + \left(Cu_B^{brine} - Cu_A^{brine}\right)}{\left(Cu_A^{vap} - Cu_A^{brine}\right)} \tag{5}$$

and by writing a similar equation based on (3) and (4) and combining it with (5), the sum is:

$$y = \frac{\left(Na_B^{brine} - Na_A^{brine}\right) \cdot \left(Cu_A^{vap} - Cu_A^{brine}\right) - \left(Cu_B^{brine} - Cu_A^{brine}\right) \cdot \left(Na_A^{vap} - Na_A^{brine}\right)}{\left(Cu_B^{vap} - Cu_B^{brine}\right) \cdot \left(Na_A^{vap} - Na_A^{brine}\right) - \left(Na_B^{vap} - Na_B^{brine}\right) \cdot \left(Cu_A^{vap} - Cu_A^{brine}\right)} \tag{6}$$

Thus, the mass fraction y of vapor in boiling assemblage B (and, consequently, also the mass fraction x of vapor in boiling assemblage A) can be calculated from two elements for which the concentrations are known for all end members of two genetically related boiling assemblages, assuming that the system is closed (i.e., there is no gain or loss of the components chosen). In perfectly closed systems these calculations should return the same values for x and y for any combination of two elements. Of course, real magmatic-hydrothermal systems are not closed but open to mass transfer (e.g., chemical evolution of the parent fluid; preferential loss of one fluid phase from the two-phase environment, such as vapor loss; deposition of one element, such as Cu). Therefore, the result from one element pair might return a different result than that from another element pair. However, if the calculations are made for a large number of element pairs (if possible comprising both vapor-fractionating and brine-fractionating elements), and if reproducible results are obtained independent of which elements are combined with each other, it is reasonable to infer that a good estimate of the mass fraction of vapor in the parent fluid can be made.
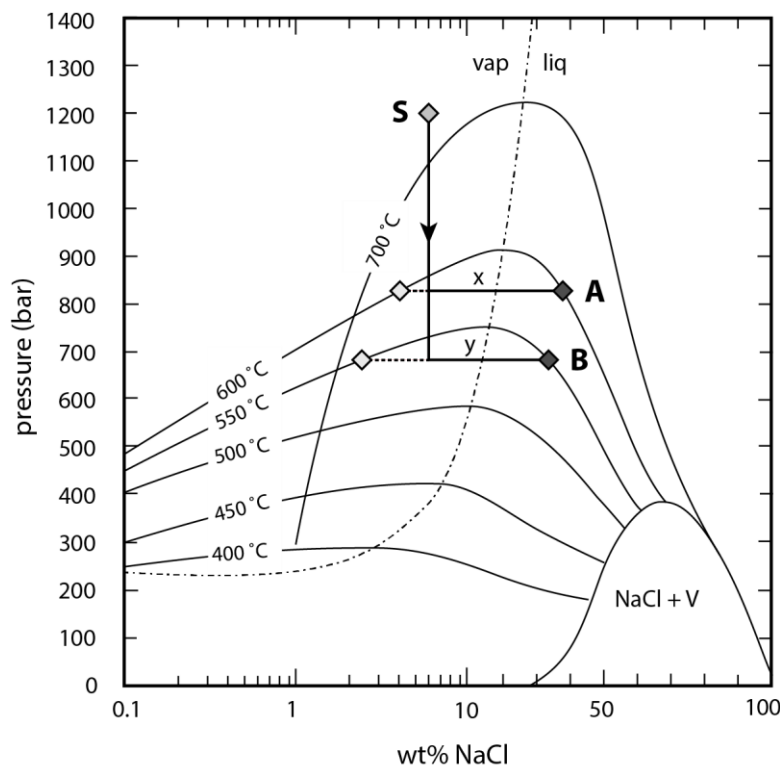
Figure 17. P-X-diagram of the system H2O-NaCl, showing the limits of the vapor–brine immiscibility field at various temperatures, plus the stability field of NaClsolid + vapor. Cooling and decompression of a 5 wt% NaCl salinity fluid (S) from 700 ⬚C and 1200 bar produces boiling assemblage A at 600 ⬚C and 820 bar and boiling assemblage B at 550 ⬚C and 680 bar. The corresponding mass fractions of vapor are marked as x and y, respectively. Note that the x-axis changes from logarithmic to linear scale at 10 wt% NaCl, which precludes the mass fractions of vapor and brine to be read out by simple geometric means.

Data from intrusions in which both single-phase fluids and several boiling assemblages (i.e., before and after intersection of the solvus) were analyzed can be used to test this approach (e.g., for the Rito del Medio Pluton, the Stronghold Granite and the Mole Granite). Of these, the most extensive and coherent data set, including three boiling assemblages and seven single-phase fluids, is available from the barren Rito del Medio Pluton. Two of the boiling assemblages (Rito8-C and Rito8-D) and five single-phase fluids (Rito8-A, B, E, F, G) were measured in the same crystal, providing the opportunity to check whether the calculation method works at the scale of an individual miarolitic cavity. Seven elements (Na, Zn, K, Mn, Cu, Pb and Cs) could be analyzed in all end members of the two boiling assemblages, permitting 21 different element combinations for the calculation of

22

the mass fractions of x and y. The results are shown in both numerical and graphical form in Figure 18. Despite some scatter there is a prominent peak at high vapor mass fractions (x=0.95 and y=1.0), suggesting that the composition of the theoretical parent fluid was almost identical to that of the vapor phase in the boiling assemblages. For some element combinations (e.g., Pb-Zn, Pb-Cs) the x and y values are calculated to be > 1, which means that a small amount of brine would have to be removed from one assemblage (or from both) to obtain a common parental fluid. This can be due to two reasons: either the system was not perfectly closed (i.e., the two boiling assemblages were not derived from exactly the same parent fluid) or a small amount of brine was trapped along with vapor in one (or both) boiling assemblage(s) (e.g., Bodnar et al., 1985). Nevertheless, the composition calculated for the hypothetical bulk fluid (on the basis of x=0.95 or y=1.0) agrees well with that of the real single-phase fluid in Rito8-E (Fig. 19a; correlation coefficient r = 0.995) analyzed in this crystal, and slightly less well with that of more fractionated single-phase fluid inclusions from this sample (r = 0.943-0.987; not shown in Fig. 19). The fact that the best match between calculated and observed fluid composition is obtained for the *least* fractionated fluid of Rito8-E implies that the cavity changed from an approximately closed system to an open system after the two-phase field was reached (if it remained closed the best fit would be expected for the *most* fractionated single-phase fluid of Rito8-G).
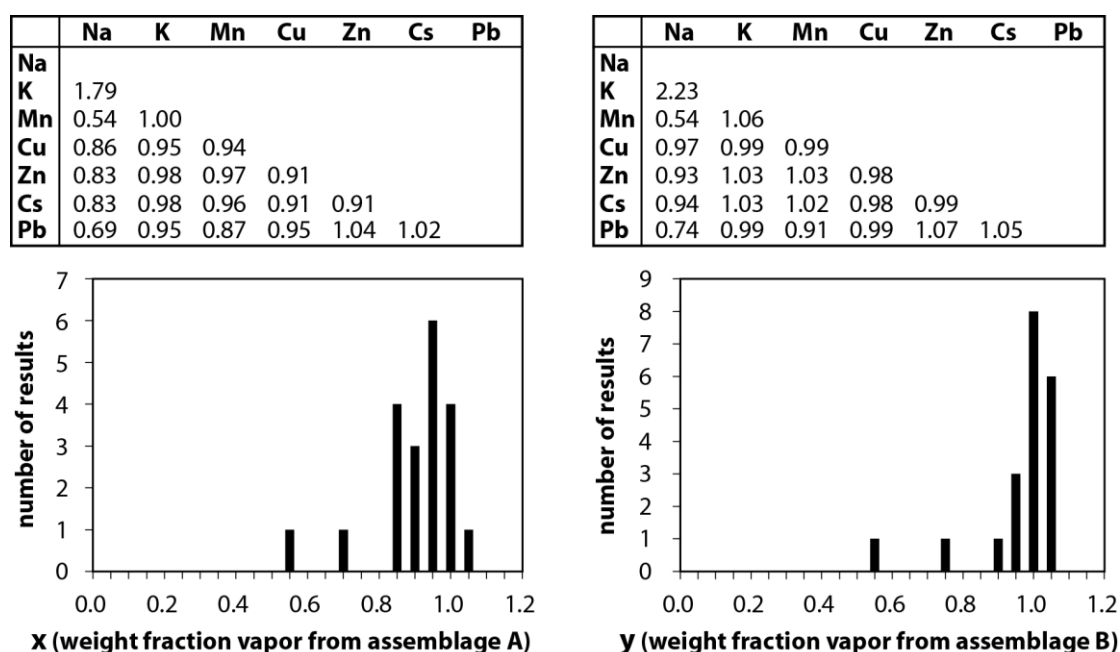
	Na	K	Mn	Cu	Zn	Cs	Pb
Na							
K	1.79						
Mn	0.54	1.00					
Cu	0.86	0.95	0.94				
Zn	0.83	0.98	0.97	0.91			
Cs	0.83	0.98	0.96	0.91	0.91		
Pb	0.69	0.95	0.87	0.95	1.04	1.02	

	Na	K	Mn	Cu	Zn	Cs	Pb
Na							
K	2.23						
Mn	0.54	1.06					
Cu	0.97	0.99	0.99				
Zn	0.93	1.03	1.03	0.98			
Cs	0.94	1.03	1.02	0.98	0.99		
Pb	0.74	0.99	0.91	0.99	1.07	1.05	

(Left chart: y-axis "number of results" 0–7; x-axis "x (weight fraction vapor from assemblage A)" 0.0–1.2)

(Right chart: y-axis "number of results" 0–9; x-axis "y (weight fraction vapor from assemblage B)" 0.0–1.2)

Figure 18. Vapor fraction in a calculated single-phase fluid released from the Rito del Medio Pluton, modeled based on element concentrations in vapor and brine inclusions on the boiling assemblages "Rito 8C" and "Rito 8D". Each element combination returns a value for the mass fraction of vapor in assemblage A ("Rito 8C"; numbers in the upper left) or the mass fraction of vapor in assemblage B ("Rito 8D"; numbers in the upper right) that would be present in the calculated single-phase fluid. The lower part of the figure is a statistical visualization of the numerical results listed above, demonstrating that most element combinations return a high fraction of vapor in the calculated single-phase fluid. See text for further explanation.

To check whether this approach works also at larger scales we can do a similar calculation with boiling assemblages measured in two different cavities of this pluton (e.g., Rito8-D and Rito5-B). The composition of the hypothetical bulk fluid calculated on this basis is very similar to that of real single-phase fluids in either of the two cavities (Fig. 19b, c), suggesting that the method is also robust in this case. An even more challenging test can be made with the data from the Mole Granite by using boiling assemblages from two different vein-type deposits (Gold1B and Wolf12A, for example) and comparing the calculated bulk fluid with single-phase fluids trapped in miarolitic quartz Leno2 (Fig. 19d). Considering the fact that these occurrences are spaced kilometers apart and

probably did not form exactly at the same time, the agreement between calculated and real fluid composition is remarkably good.
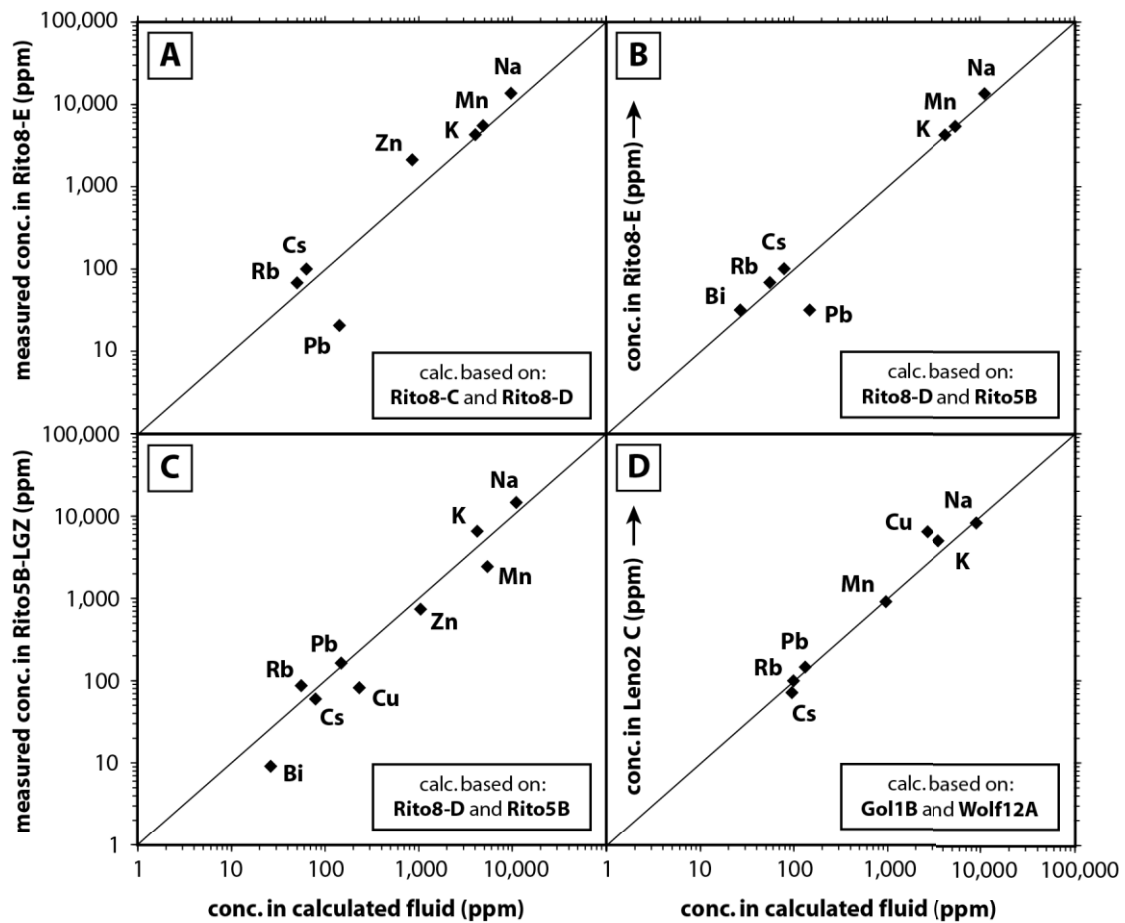

Figure 19. Comparison of the composition of hypothetical bulk fluids calculated from subsolidus boiling assemblages in the Rito del Medio Pluton, New Mexico, and the Mole Granite, Australia, with that of actually occurring, single-phase fluids in these plutons. **A.** Hypothetical bulk fluid calculated from boiling assemblages "Rito8-C" and "Rito8-D" versus single-phase fluid "Rito8-E" in the Rito del Medio Pluton. **B.** Hypothetical bulk fluid calculated from boiling assemblages "Rito8-D" and "Rito5-B" versus single-phase fluid "Rito8-E". **C.** Hypothetical bulk fluid calculated from boiling assemblages "Rito8-D" and "Rito5-B" versus single-phase fluid "Rito5-B LGZ". **D.** Hypothetical bulk fluid calculated from boiling assemblages "Gold1B" and "Wolf12A" versus single-phase fluid "Leno2" in the Mole Granite.

This calculation has been applied to those occurrences in Table 1 where several boiling assemblages but no single-phase, parent fluids were identified (i.e., Bajo de la Alumbrera, Cave Peak and Santa Rita). Two representative histograms of each of these occurrences are shown in Figure 20. At Bajo de la Alumbrera and Cave Peak the calculations always result in a prominent peak at around 1 (or slightly higher), independent of which boiling assemblages are combined with each other. This suggests that the bulk fluid was dominated by vapor also in these systems. At Santa Rita, on the other hand, no clear picture emerges, suggesting that the analyzed boiling assemblages did not originate from a common parent fluid. This is plausible, as most fluids analyzed from Santa Rita exsolved directly from the melt, as noted above, and thus the fluid composition likely changed with increasing degree of magma crystallization. However, it does not explain why the method works in the other locations, because the composition of the magmatic parent fluids must also have changed with increasing crystallization and degree of magma fractionation in these locations. One explanation might be that the boiling assemblages at Santa Rita formed at magmatic temperatures and ductile conditions, when the miarolitic cavity behaved as a locally closed system, whereas the boiling assemblages from the other localities formed at subsolidus conditions, where the presence of brittle fractures allowed

fluid to be transported over much larger distances. Therefore, the composition of fluids trapped under subsolidus conditions is expected to be less affected by variable degrees of melt fractionation.

In summary, the numerical approach presented in this section provides a good constraint on the bulk composition of the parent fluid in two out of the seven occurrences in which no single-phase fluid could be identified with certainty. In the remaining five occurrences (Cuasso al Monte, Mt. Malosa, Santa Rita, Grasberg and Capitan Mountains), the method could either not be applied (because not enough data from boiling assemblages are available), or it did not return useful results because both vapor and brine exsolved directly from the melt (i.e., Santa Rita).
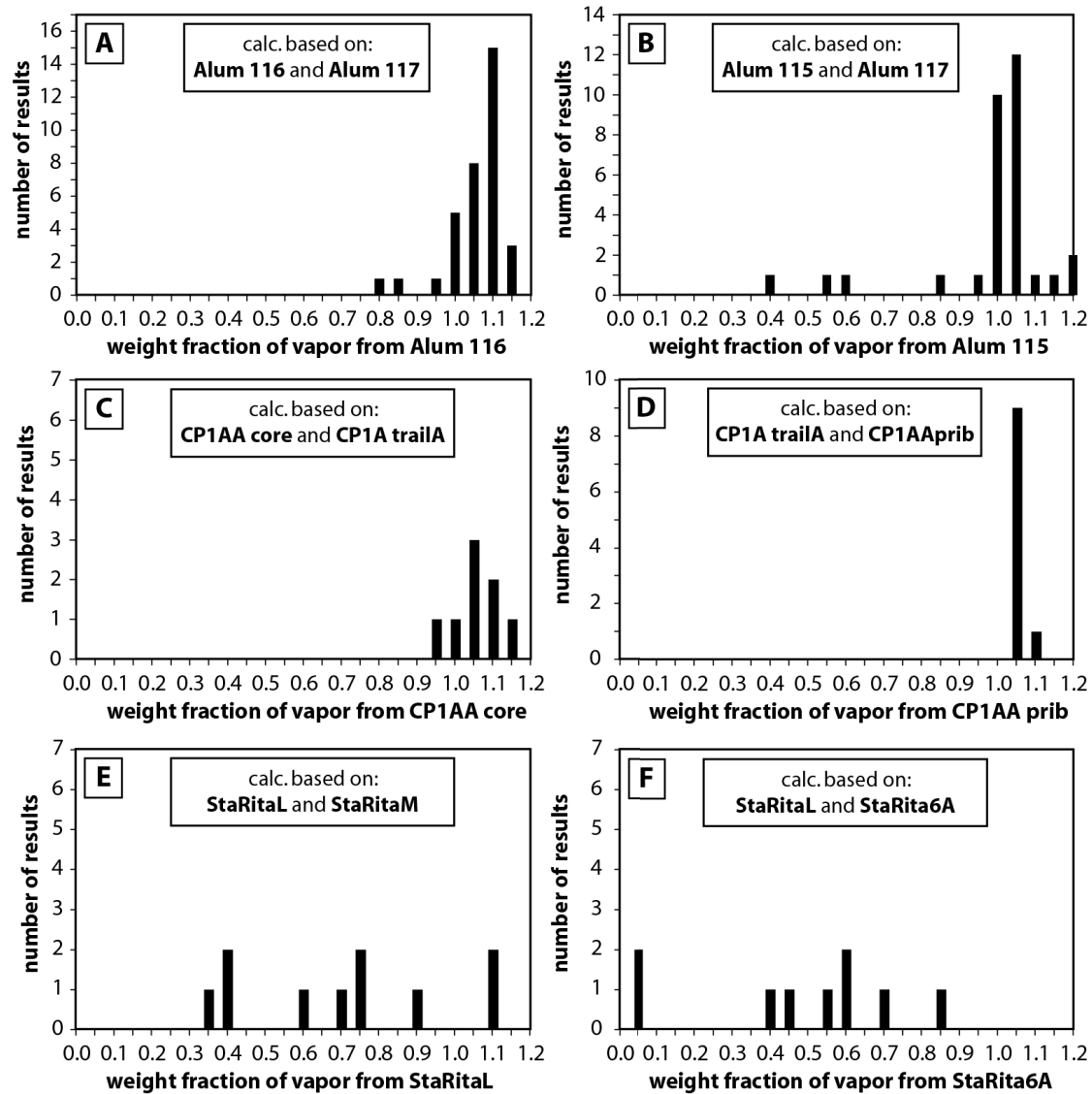
Figure 20. Vapor fractions (by weight) in hypothetical bulk fluids calculated from subsolidus assemblages in intrusions in which no parental, single-phase fluid was found. **A, B**. Results for Alumbrera, Argentina, based on LA-ICP-MS data from Ulrich et al. (2002). **C, D**. Results for Cave Peak, Texas. **E, F**. Results for Santa Rita, New Mexico. The results for Alumbrera and Cave Peak indicate that the hypothetical bulk fluid is dominated by vapor, whereas at Santa Rita no statistical maximum can be discerned. Vapor fractions greater than unity suggest that a small amount of brine has to be subtracted from one (or both) boiling assemblage(s) to obtain a common parental fluid.

5. Identifying the Most Representative Fluid of a Pluton

The data presented in the previous sections demonstrate that the salinity and metal content of single-phase fluids derived from crystallizing magmas varied significantly as a function of the degree of melt fractionation, as predicted by numerical models of magma crystallization at fluid-saturated conditions (e.g., Candela, 1989; Nakano and Urabe, 1989; Cline and Bodnar, 1991; Candela and Piccoli, 1998; based on experimental data of, e.g., Holland, 1972; Kilinc and Burnham, 1972; Candela and Holland, 1984; Urabe, 1985; Shinohara et al., 1989). The numerical models suggest that in plutons crystallizing at shallow levels (<1.3 kbar: Cline and Bodnar, 1991) the salinity of the exsolving fluid increases with increasing degree of magma crystallization, whereas in plutons crystallizing at deeper levels the fluid salinity decreases with increasing degree of magma crystallization. Most of the occurrences listed in Table 1 formed at <1.3 kbar, hence the concentrations of chlorine-complexed elements should be highest in the fluids exsolving at high degrees of crystallization. According to the models of Candela (1989), Cline and Bodnar (1991) and Candela and Piccoli (1998) the maximum concentration of chlorine-complexed metals in the fluid is reached between 80 and 98 % crystallinity, depending on confining pressure and Cl/H_2O ratio in the starting magma. The concentrations of the non-chloride-complexed elements Mo and W are also expected to be highest in the late exsolving fluids because they behave incompatibly with respect to both the exsolving fluids and the crystallizing minerals, and thus become enriched in the residual melt (Candela, 1989). However, at some point during the crystallization of the last few percent of magma the mass of as yet unexsolved fluid becomes so small that it is unlikely that economic mineralization could be produced by this fluid any more. Thus, the fluids with highest mineralization potential (i.e., with both high metal content and significant mass) probably exsolved between ~80 and ~99 % crystallinity. Miarolitic cavities seem to have formed at >90 % crystallinity, hence fluid inclusions trapped in miarolitic quartz are likely to be representative of very late fluids. Indeed, many of the single-phase magmatic fluids analyzed in miarolitic quartz contain more than 50-100 ppm Cs (which is the maximum Cs content of fractionated magmatic rocks of considerable volume; i.e., topaz rhyolites: Christiansen et al., 1983), suggesting that they exsolved during the final stage where the amount of residual fluid may have been too small to produce economic mineralization. For this reason we regard the *least* fractionated single-phase fluid (i.e., the one with the lowest Cs concentration) found in miarolitic quartz as most representative with regard to the mineralization potential.

Miarolitic cavities commonly are concentrated in the uppermost or outermost 100-200 m of a given pluton, which is also the location of intrusion-hosted vein- and greisen-type ore deposits. Because the host carapace had to be fully (or nearly fully) crystallized before these types of deposits formed, they cannot have formed earlier than miarolitic cavities occurring in the same rock portion. Hence, the fluids responsible for the formation of intrusion-hosted vein- and greisen-type deposits (but not necessarily for the formation of porphyry deposits) are likely to have passed through the miarolitic cavities and thereby have become trapped in miarolitic quartz. The Mole Granite, with fluid inclusion data available from both miarolitic cavities and vein-type deposits, can be used to test this hypothesis. It should be noted, however, that only fluids trapped at subsolidus conditions can be used for this comparison because no single-phase fluids have been found in the mineralized veins of this intrusion. A comparison between early (400-600 °C) brine inclusions in Leno2 with early brine inclusions in five different vein and greisen-type Sn, W and/or Bi-Au deposits within the Mole Granite reveals no systematic compositional differences (Fig. 21). The same is true for the composition of corresponding vapor inclusions (Appendix 1). Thus, at least in the Mole Granite, the concept of using fluid inclusions from miarolitic quartz as a proxy for the potentially mineralizing fluids appears to be valid.
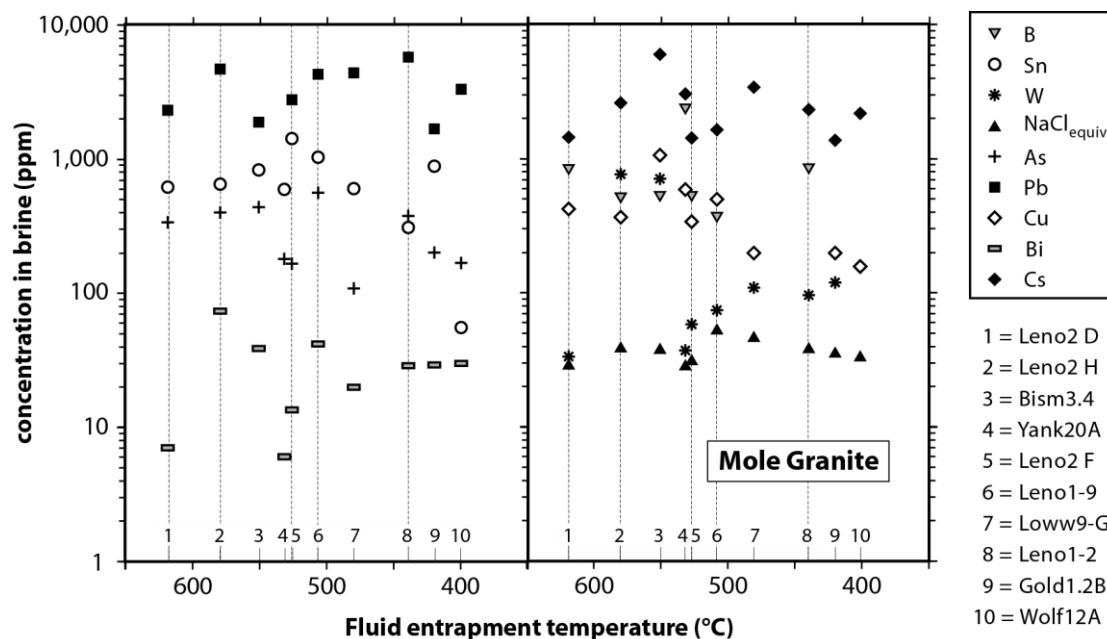
Figure 21. Comparison of the composition of medium to high-temperature brine inclusions trapped in miarolitic quartz of the Mole Granite ("Leno1", "Leno2"; marked by stippled lines) with that of similar temperature brine inclusions analyzed from mineralized veins within the same intrusion. No systematic compositional differences between the two data sets are evident, suggesting that brine inclusions in miarolitic quartz are representative of the potentially mineralizing fluids.

6. Fluid Composition Versus Deposit Type

6.1. Least fractionated low-salinity fluid

Table 2 compares the metal content of the highest temperature and/or least fractionated single-phase fluid (or, if no single-phase fluid was available, from the least fractionated vapor) from each of the occurrences listed in Table 1, except for Cuasso al Monte for which no data on the vapor phase is available. In the case of the Mole Granite we report two compositions to differentiate between fluids associated with Sn deposits and fluids associated with W deposits, the latter spatially related to rocks that are more fractionated than those associated with Sn deposits (Audétat et al., 2000a). If the concentration of a given element in the least fractionated fluid was not known or seemed erratic, it was estimated based on the trend displayed by more fractionated fluids. The values listed in Table 2 should be regarded only as approximate indications, as they strongly depend on sample coverage. The values listed for the Rito del Medio Pluton, for example, would be up to an order of magnitude higher if the least fractionated fluid (Rito5B-2LGZ; Fig. 13) was not analyzed. For Grasberg, Capitan Mountains, Baveno and Ehrenfriedersdorf only very few data are available; therefore, the values listed for these occurrences may be less representative than those listed for other localities.

The least fractionated fluids analyzed from Baveno, Stronghold, Ehrenfriedersdorf and the W (Bi)-mineralized part of the Mole Granite contain more than 100 ppm Cs and thus might represent a very late, volumetrically minor fluid phase. On the other hand, the fact that the metal content of these fluids reflects fairly well the type and degree of associated mineralization may be regarded as evidence that even the most fractionated fluids listed in Table 2 may have been volumetrically significant enough to contribute to the mineralization. A different source of uncertainty is related to those occurrences in which the earliest fluid found is two-phase, because vapor–brine partitioning leads to a depletion of Cs and most other elements (except for Cu, As, Au, B ± Sb, Li) in the vapor phase. Due to the fact that the solvus commonly is intersected on the vapor limb, this effect will be significant only if the analyzed fluid was trapped at significantly lower

27

Table 2. Composition of the highest-temperature and/or least fractionated low-salinity fluid found at each location

Mineralization	Locality	Fluid state[1]	NaClequiv (wt%)	Cs (ppm)	Cu (ppm)	Mo (ppm)	Sn (ppm)	W (ppm)	Ce (ppm)	Pb (ppm)	Zn (ppm)	Remarks
barren	Rito del Medio	S	4,5	6	300	70	<30	10	<1	70	<500	Rito5B 2LGZ (1), (2)
barren	Cañada Pinabete	S	3,9	20	100	<50	<90	10	<2	60	400	Cana12 in (2)
barren[2]	Baveno[3]	S	5,9	200	300	80	90	60	9	300	1000	Bav13 (15)
barren[2]	Mt. Malosa[3]	T	11,1	40	200	10	300	100	10	600	1000	Mal02i (15)
(Zn-Pb-Cu)	Stronghold	S	6,2	100	1000	30	60	70	<3	200	700	Stro15 FI1, 2 (1)
Cu (Mo-Au)	Santa Rita	T	20,1	10	8000	5	<100	20	<7	400	3000	StaRitaL, M (1)
Cu-Au-Mo	Alumbrera	S?	3.4-5.7	5	20000	n.a.	<100[4]	20	3	200	1000	# 31, 32, 40, 41, 42 in (3)
Cu-Au (Mo-Ag-Pb-Zn)	Bingham	T	5 (?)	5	3000	50	<90	30	n.a.	300	400	Single-phase fluid in (9)
Cu (Mo-Ag-Zn-Au)	Butte	S	2,7	6	4000	7	<30	10	n.a.	20	100	#2756 in (7), (9)
Cu-Au (Ag)	Grasberg[3]	T	7,4	4	3000	50	10	<5	n.a.	300	1000	(8), (9)
Cu (Mo)	El Teniente	S	12-13	40	10000	70	80	20	n.a.	200	2000	Calculated input fluid (16)
Mo-Nb (Cu-W)	Cave Peak	T	3,1	10	20	20	20	6	<1	50	<100	CP1AAcore (1)
Mo	Questa	S	6,0	5	3000	40	40	20	n.a.	200	500	IDMHBX in (11)
Sn-W (Cu-Ag-Pb-Zn)	Mole Granite	S	3,1	70	6000	50	100	<10	<7	200	200	Leno2 A, B (1)
W (Bi)	Mole Granite	S	4,5	200	200	200	<1700	100	<10	90	<1000	Bism3.3 3-6 (13), (1)
Sn (W)	Ehrenfriedersdorf[3]	S	7.0-8.5	1000	10000	7	3000	100	2	20	2000	(15)
(Th-U-REE)	Capitan Mt.	T	2,2	10	100	n.a.	n.a.	<20	10	40	n.a.	Capi3 pheno (1)

[1] S - trapped in single-phase field; T - trapped in two-phase field; [2] occurrence of ore minerals in the miarolitic cavities (e.g., Pezzotta et al., 1999);

[3] only few data available, hence data are less likely to be representative; [4] higher values are regarded as an artefact caused by imperfect matrix correction;

(1) this study; (2) Audétat and Pettke, 2003; (3) Ulrich et al., 2002; (7) Rusk et al., 2004; (8) Ulrich et al., 1999; (9) Williams-Jones and Heinrich, 2005;

(11) Klemm et al., 2008; (13) Audétat et al., 2000a; (15) Zajacz et al., 2008; (16) Klemm et al., 2007

pressure than pressure at which the solvus was intersected, or if prolonged open-system degassing and mass loss occurred in the meantime. Thus, by choosing the fluid assemblage that was trapped at the highest temperature (which corresponds to the highest pressure in most cases), the uncertainty caused by vapor–brine partitioning should be minimized. For the reasons described above, only one significant figure is listed in Table 2, and associated uncertainties are probably a factor of two to three at least.

Despite these uncertainties it appears that the metal content of the parent aqueous fluid correlates positively with the type of mineralization: high Cu concentrations are present in the fluids analyzed from porphyry Cu deposits, high Sn and W contents in those analyzed from Sn-W-mineralized intrusions, and high Ce contents in the fluids from the Th-U-REE-mineralized Capitan Pluton. However, there are some notable exceptions. Molybdenum, for example, is not particularly abundant in the fluids associated with Mo mineralization, and the fluids at Questa, the Mole Granite and Ehrenfriedersdorf contain similarly high Cu concentrations as those associated with porphyry Cu deposits. There is significant Cu-Au-Pb-Zn mineralization in the country rocks surrounding the Mole Granite (Henley et al., 1999, 2000), and although no Cu mineralization is present within the Questa Mo deposit, numerous Cu-Au-Ag-Pb-Zn deposits occur at structurally shallower levels along the Questa caldera margin (Clark and Read, 1972; Jones, 1990). In the case of Pb and Zn, no clear correlation between fluid composition and presence of Pb-Zn mineralization is observed.

The fluids analyzed from barren intrusions are not particularly metal rich compared with the metal concentrations of fluid inclusions related to mineralized deposits (i.e., Cu in the fluids related to porphyry Cu deposits, or Sn in the fluids related to Sn deposits). Exceptions are the high concentrations of Mo, Sn, W and Ce reported in some of the fluids analyzed from Baveno and Mt. Malosa, two barren intrusions; however, these two localities are famous for a large variety of rare minerals (including ore minerals) occurring in the miarolitic cavities. From Mt. Malosa, cassiterite, scheelite and many REE-bearing minerals have been described (Demartin et al., 2003; Guastoni et al., 2004), and at Bavona cassiterite, wolframates, molybdates and many REE-bearing minerals are present (Pezzotta et al., 1999). Thus, the fluids exsolving from these intrusions had the potential to produce mineralization, but apparently were not sufficiently focused to form an ore deposit.

6.2. Least fractionated brine

A similar comparison based on the composition of the highest temperature and/or least fractionated brine inclusions found at each location is presented in Table 3. For Mo, Sn, W and Ce the correlation between fluid composition and type and degree of mineralization seems to be even more distinct for high-temperature brines than in the least fractionated low-salinity fluid. Whereas none of the three highest Mo values in low-salinity fluid (Table 2) coincides with areas of economic Mo mineralization, three out of the four highest Mo values in brines (Table 3) do so. The highest Mo content in brines is reported from Grasberg, which is principally a Cu-Au porphyry deposit, although significant Mo mineralization may be present at depth (Pollard and Taylor, 2002). The number of locations at which high concentrations of Sn, W and Ce in the fluid coincide with areas of Sn, W and Ce mineralization are about the same in both low-salinity and brine fluids (Tables 2 and 3). However, the matching points are more readily discernible in the brines (Table 3) because the concentration differences in the brines are larger than in the low-salinity, parental fluids. Exceptionally high concentrations of Sn and W are reported from the brines at Cuasso al Monte, which is another locality known for a large variety of rare minerals (including cassiterite and wolframates) occurring within the miarolitic cavities

Table 3. Composition of the highest-temperature and/or least fractionated brine found at each location

Mineralization	Locality	NaClequiv (wt%)	Cs (ppm)	Cu (ppm)	Mo (ppm)	Sn (ppm)	W (ppm)	Ce (ppm)	Pb (ppm)	Zn (ppm)	Remarks
barren	Rito del Medio	26	1000	2000	90	<300	50	<8	2000	20000	Rito8-D (1), (2)
barren	Cañada Pinabete	40	80	80	10	<40	90	100	3000	8000	Cana2 in (2)
barren[1]	Cuasso al Monte[2]	53-69	1000	200	6	1000	1000	20	3000	20000	K/Na=0.4 (15)
barren[1]	Mt. Malosa[2]	32-34	100	40	5	50	20	1	3000	7000	Mal25as1 (15)
(Zn-Pb-Cu)	Stronghold	29	4000	100	<10	50	70	<2	5000	9000	Stro15B TB 1-4 (1)
Cu (Mo-Au)	Santa Rita	33	10	2000	10	20	<70	20	800	3000	StaRitaM (1)
Cu-Au-Mo	Alumbrera	60	50	3000	60	<200[3]	10	5	4000	10000	BLA in (3)
Cu-Au (Mo-Ag-Pb-Zn)	Bingham	44	30	7000	100	<50	100	n.a.	3000	3000	(5), (6), (9)
Cu (Mo-Ag-Zn-Au)	Butte	–	–	–	–	–	–	–	–	–	highly variable
Cu-Au (Ag)	Grasberg[2]	73	70	3000	600	70	50	n.a.	5000	10000	(6), (8), (9)
Cu (Mo)	El Teniente	37-48	120	9000	20	40	40	n.a.	1000	5000	B2-1 in (17)
Mo-Nb (Cu-W)	Cave Peak	38	100	200	400	100	300	200	800	1000	CP1AAcore (1)
Mo	Questa	38	20	4000	200	30	80	n.a.	2000	4000	BMHBX in (11)
Sn-W (Cu-Ag-Pb-Zn)	Mole Granite	28	2000	400	<10	600	30	5	2000	4000	Leno2 D, H (1)
W (Bi)	Mole Granite	37	6000	1000	4	800	700	10	2000	5000	Bism3.4 (13), (1)
Sn (W)	Ehrenfriedersdorf[2]	52	600	b.d.	n.a.	400	b.d.	n.a.	n.a.	30	inclusion 1 in (16)
(Th-U-REE)	Capitan Mt.	73	70	200	80	60	30	300	500	3000	Capi MTE (1)

[1] occurrence of ore minerals in the miarolitic cavities (e.g., Pezzotta et al., 1999). [2] only few data available, hence data are less likely to be representative;

[3] Higher values are regarded as an artefact caused by imperfect matrix correction; b.d. – below detection (detection limit not specified); n.a. – not analyzed;

(1) this study; (2) Audétat and Pettke, 2003; (3) Ulrich et al., 2002; (5) Landtwing et al., 2005; (6) Heinrich et al., 1999; (8) Ulrich et al., 1999; (9) Williams-Jones and Heinrich, 2005; (11) Klemm et al., 2008; (13) Audétat et al., 2000a; (15) Zajacz et al., 2008; (16) Rickers et al., 2006; (17) Klemm et al., 2007

(Pezzotta et al., 1999). The high concentrations of Sn, W and Ce in early brines analyzed from Cave Peak are compatible with the presence of cassiterite, huebnerite and yttrofluorite (containing 1 wt% CeO) in the mineralization. Furthermore, the same brine inclusions contain 60 to 100 ppm Nb, which is significantly larger than the Nb content of high-temperature brine inclusions at other localities (10 ppm at Rito del Medio Pluton; 3 ppm at Mt. Malosa; 20 ppm at Santa Rita; 2 ppm at Mole Granite); this is consistent with the presence of major niobium mineralization at Cave Peak (Nb is not listed in Appendix 1 because only few data are available). The degree of correlation between Cu concentrations in high-temperature brines and sites of Cu mineralization is similar to that observed for the low-salinity, parental fluids. For Pb and Zn there is again no correlation with localities of Pb-Zn mineralization; in fact, the highest Zn concentrations are present in the brines from the barren Rito del Medio pluton and from Cuasso al Monte, implying that factors other than the metal content of the fluid were responsible for the failure of these intrusions to produce economic Pb and Zn mineralization.

It is not evident why the correlation between the concentrations of Mo, Sn, W and Ce in the fluid and type and degree of mineralization is more apparent in the brines than in the low-salinity fluids. If it were due to differences in the vapor-brine partition coefficients it would imply that these partition coefficients were systematically lower in the mineralized areas. Unfortunately, the available data are too limited to test this hypothesis. Another possibility is that the metal content of the brines was affected to variable degrees by fluid–mineral interactions at subsolidus conditions.

7. Controls on the Mineralization Potential of Magma Systems

Magmatic-hydrothermal ore deposits result from a large number of processes operating at different levels within the crust and the underlying mantle. Major factors that are regarded to be essential in the formation of these deposits include the formation of an upper crustal magma chamber, fractional crystallization of mafic and felsic magmas, exsolution of aqueous fluids, fluid–mineral interactions at subsolidus conditions, focusing of aqueous fluids into a confined volume, vapor-brine immiscibility, and the precipitation of ore minerals (e.g., Burnham, 1967, 1979, 1997; Ishihara and Takenuchi, 1980; Taylor and Strong, 1988; Whitney and Naldrett, 1989; Stein and Hannah, 1990; Hedenquist and Lowenstern, 1994; Hedenquist and Richards, 1998). The order in which these processes were listed corresponds to an approximate sequence of events at a given point in the magmatic-hydrothermal system or, at a given time, their position in the system from deep to shallow. Given this model and the data presented in the previous sections we are now able to discuss whether fundamental differences between barren and mineralized intrusions exist, and if so, at which stages the most important processes for mineralization occurred. The most logical approach to do this is to track the evolution back step by step, investigating at each step whether the conditions in mineralized intrusions were systematically different from those in barren intrusions.

Starting at the final stage of precipitation of ore minerals we can ask whether barren intrusions may be barren simply because of a lack of ore precipitation. Precipitation of ore minerals from hydrothermal solutions is triggered by processes including cooling, decompression, chemical reaction with the host rock, and fluid mixing (e.g., Robb, 2005; Seward and Barnes, 1997). For each metal and physicochemical environment, a different mechanism may be the most efficient metal-precipitation process. It appears that mixing between intrusion-derived fluid and surrounding groundwater was responsible for the formation of certain high-grade Sn deposits (Audétat et al., 1998, 2000b), whereas fluid cooling seems to have been a key driving factor for Cu and Mo precipitation in porphyry-type deposits (e.g., Redmond et al., 2004; Landtwing et al., 2005; Klemm et al., 2007, 2008). Metal precipitation is commonly highly selective, resulting in system-scale metal zonation and/or local metal precipitation sequences (i.e., telescoping) in individual veins.

Of the four main mechanisms of ore precipitation, cooling and decompression of magmatic-hydrothermal fluids can be expected to occur to the same extent in barren and mineralized intrusions, unless they were emplaced at different depths. Emplacement at different depths, however, does not seem to be the case. There might be a maximum depth at which magmatic-hydrothermal ore deposits can form (10 km according to Uchida et al., 2007), but above this depth both barren and mineralized intrusions commonly are emplaced at similar levels. Fluid mixing and chemical reaction with the host rock certainly exert some control, but there are numerous cases in which barren and mineralized intrusions occur next to each other in the same lithology. Therefore, we do not regard the stage of ore precipitation to be the dominant factor in controlling whether an intrusion is related to mineralization or not. However, selective metal precipitation certainly has a large influence on the ore metal ratios, explaining how an essentially pure Mo deposit could form at Questa and an essentially pure Sn deposit in the Yankee Lode of the Mole Granite, despite concentrations of Cu, Pb and Zn in the input fluids up to one order of magnitude higher than those of Mo and Sn, respectively (Audétat et al., 1998; 2000b; Klemm et al., 2008; Tables 2 and 3, Appendix 1). On the other hand, selective mineral precipitation cannot have been the only factor controlling the ore metal ratios, because for some elements there is a distinct correlation between ore type and the composition of the magmatic parent fluid (Table 2).

Fluid immiscibility may occur during the magmatic stage (if two fluids exsolve from the melt simultaneously), but at most localities considered in this study the fluid solvus was intersected after the surrounding magma was fully solidified. Fluid immiscibility and related vapor–brine partitioning of ore metals may affect the mineralization process in several ways, including: (i) ore precipitation as a direct consequence of fluid boiling and associated loss of H_2S (amongst other things), (ii) physical separation of chemically contrasting fluids, leading to system-scale metal zonation, and (iii) accumulation of chlorine-complexed metals in residual brine. The first process was shown to be an efficient mechanism for the precipitation of gold in shallow epithermal deposits and in deeper orogenic deposits, where vapor exsolves from liquid-dominated fluids (e.g., Drummond and Ohmoto, 1985). In the environment of porphyry and intrusion related vein- and greisen-type mineralization, however, where the field of immiscibility is approached from the vapor side rather than from the liquid-rich side (e.g., Henley and McNabb, 1978; Burnham, 1979; Shinohara and Hedenquist, 1997; Hedenquist et al., 1998; Audétat and Pettke, 2003; Rusk et al., 2004; Redmond et al., 2004; Landtwing et al., 2005; Williams-Jones and Heinrich, 2005; Klemm et al., 2007, 2008; this study), the physical process of vapor-brine immiscibility probably does not lead to metal precipitation. In fact, in all occurrences in which the timing of ore precipitation relative to the intersection of the parent fluid with its solvus could be reconstructed (Bajo de la Alumbrera, Bingham, Butte, Cave Peak, Questa, Mole Granite), ore precipitation occurred either earlier or later than the onset of aqueous fluid immiscibility (Audétat et al., 1998, 2000b; Ulrich et al., 2002; Rusk et al., 2004; Redmond et al., 2004; Landtwing et al., 2005; this study).

Vapor–brine immiscibility leads to contrasting metal partitioning between the two phases, with chlorine-complexed elements fractionating into the brine, and S, Cu, As, Au, B (± Li, Sb) fractionating into the vapor phase (e.g., Heinrich et al., 1999; Williams-Jones and Heinrich, 2005). Physical separation of the two fluid phases can thus result in a spatial metal zonation. Removal of Fe-rich brine from S-, Cu-, and Au-bearing vapor was invoked to explain the formation of epithermal Au (-Cu) deposits above porphyry Cu (-Mo, Au) deposits (Heinrich et al., 2004, 2005), and escape of Cu-rich vapor to explain the lack of copper mineralization at the Questa porphyry Mo deposit (Klemm et al., 2008) and at the Refugio and other deposits of the Maricunga Au porphyry deposits, Chile (Muntean and Einaudi, 2001). High rates of metal discharges during volcanic eruptions (e.g., Hedenquist and Lowenstern, 1994; Hedenquist, 1995) and mass balance constraints from extinct systems (Halter et al., 2005) indicate that the overall efficiency of metal precipitation in

porphyry Cu systems may be rather small, with more metal being lost by dispersion than ultimately accumulated in the deposits.

Condensation of brine from a low-density parental fluid and its accumulation at depth could thus be an efficient mechanism to concentrate chlorine-complexed metals in a small rock volume, promoting the opportunity to form an ore deposit at the deeper levels of magmatic-hydrothermal systems. The following two factors would contribute independently to this scenario: (i) the solubilities of many metals are higher in the brine than in vapor (e.g., Sn, W, Mo, REE, but not Cu and Au), and (ii) brines occupy a much smaller volume than the same mass of vapor, thereby increasing the likelihood of metal precipitation in a small rock volume.

Several lines of evidence suggest that brines indeed played a crucial role in the formation of many types of magmatic-hydrothermal ore deposits, despite the fact that they represented only a small fraction of the total fluid that exsolved from the associated intrusions. First, for Mo, Sn, W and Ce the correlation between fluid composition and type of mineralization is greater in the brines than in the low-salinity fluids. Second, intrusion-scale mapping by John (1989) and Ratajeski and Campbell (1994) document a clear correlation between the abundance of brine inclusions (relative to other types of fluid inclusions) and the occurrence of Cu, Pb, Zn, Ag and REE mineralization. John (1989) noted that most hydrothermal mineralization is associated spatially with parts of the intrusions where high-salinity fluids are present; Ratajeski and Campbell (1994) found that vapor-rich inclusions are abundant in quartz phenocrysts but extremely scarce in vein quartz. Although the relative abundance of vapor versus brine inclusions trapped in a given sample is not necessarily a good monitor of the relative abundances of the corresponding fluid phases (because of differences in their wetting properties, which can lead to different probabilities of fluid entrapment: e.g., Roedder, 1984), it nevertheless is difficult to imagine how veins in the Capitan Pluton, in which vapor inclusions are virtually absent, could have formed by anything other than a brine-dominated fluid.

Further evidence of a major role for brines in the formation of some magmatic-hydrothermal ore deposits comes from fluid evolution trends recorded in individual quartz crystals from vein deposits within the Mole Granite. As shown by Sun and Eadington (1987) and Audétat et al. (1998, 2000b), stages of Sn, W and Bi ore formation in this intrusion were caused by mixing between magma-derived and meteoric fluids and are recorded in the brine by Sn, W and Bi concentrations that decrease more sharply than those of non-precipitating elements such as Na, K, Cs and Pb (the latter decreasing due to the dilution by meteoric water). At the same time, the concentrations of the vapor-fractionating elements Cu, B and Li in the brine *increased* relative to those of Na, K, Cs and Pb. This observation is incompatible with vapor having been the dominant phase in these veins, because in this case the concentrations of Cu, B and Li should have decreased in both vapor and brine (in the vapor due to the addition of meteoric water, and in the brine because it can only mimic the compositional evolution of the vapor if the brine/vapor mass ratio is small). Rather, this pattern suggests that the ore-forming fluid was dominated by brine and that the admixed meteoric water was enriched in Cu, B and Li due to condensation of vapor into it. The fluid evolution in the veins of the Mole Granite can therefore be visualized as follows (Fig. 22): (1) exsolution of a vapor-rich, single-phase fluid from the crystallizing magma, (2) condensation of brine from this fluid, (3) accumulation of brine in the lower portions of the vein system, while vapor escapes upward and is condensed by meteoric water, and (4) incursion of the meteoric water into the pluton interior, causing ore precipitation upon mixing with brine. This model is similar to that proposed for Questa, where it was suggested that sequestering of Mo by brine and concomitant escape of Cu-rich vapor was one of the two reasons (the other being selective metal precipitation) why virtually no Cu is present in the deposit despite a Cu/Mo ratio of about 70 by weight in the single-phase bulk fluid (Klemm et al., 2008).

Evidence for accumulation of brine is present also in sample CP1 (Fig. 10) from Cave Peak, where the abundance of brine inclusions relative to vapor inclusions increases sharply from primary clusters in the core to pseudosecondary trails that were trapped at the time of mineralization.
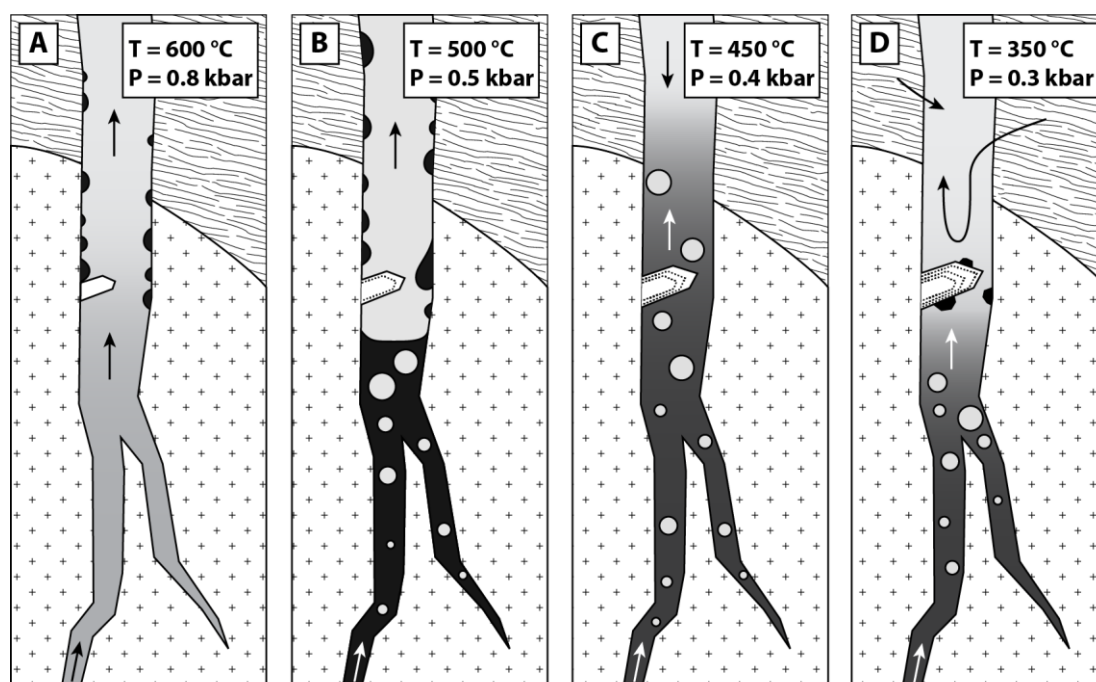

Figure 22. Schematic illustration of the fluid evolution in Sn-W-mineralized veins in the Mole Granite, Australia. **A.** Exsolution of a single-phase, magmatic fluid ($\sim$ 5 wt% NaCl$_{equiv}$) in the deeper parts of the intrusion, which condenses a small amount of brine upon its rise to higher levels. **B.** Prolonged condensation of brine and escape of vapor to higher levels leads to accumulation of brine in the deeper parts of the vein system. **C, D.** Further cooling of the pluton is accompanied by the incursion of meteoric water into the now brine-dominated vein system, causing Sn-W ore precipitation at the mixing front between meteoric water and metal-rich brine (e.g., black crystals on the quartz crystal in D). Approximate pressure and temperature conditions refer to the position of the quartz crystal in the central part of the vein system.

The degree to which brines are involved in the formation of porphyry Cu (-Au) deposits cannot be determined with certainty at this stage, but a major role appears less likely because the high vapor/brine mass ratio coupled with high vapor/brine partition coefficients requires that ≥90 percent of the Cu and Au in these systems was transported by the vapor phase (e.g., Hedenquist et al., 1993; Redmond et al., 2004; Landtwing et al., 2005; Williams-Jones and Heinrich, 2005; Klemm et al., 2007). Furthermore, textural relationships in mineralized veins of Bingham (described in Landtwing et al., 2005) have been interpreted to reflect Cu precipitation from cooling vapor (Williams-Jones and Heinrich, 2005). On the other hand, in porphyry Cu deposits the abundance of brine inclusions is similar to that of vapor inclusions, and brine inclusions seem to be particularly abundant in the area of mineralization (e.g., Roedder, 1971; Moore and Nash, 1974; Eastoe, 1982; Bodnar, 1995; Roedder and Bodnar, 1997).

In summary, the combined evidence strongly suggests that fluid immiscibility and associated condensation of brine played a central role in the formation of Sn, W, Mo and REE deposits, but probably to a smaller degree in the formation of porphyry Cu-(Au) deposits. Again, the fact that a distinct correlation between deposit type and metal composition of fluid exists in the single-phase parent fluids (Table 2) implies that processes related to vapor-brine immiscibility were not the only factors controlling the mineralization potential, but that earlier stages must have played an important role as well.

The transition from magmatic to subsolidus conditions includes some processes that are still poorly understood. Minerals that were stable under magmatic conditions may become unstable and transform into other minerals, causing a redistribution of metals and ligands between minerals and exsolved aqueous fluids. For example, magmatic sulfides decompose to Fe-oxides during degassing and cooling of a magma body, thereby releasing sulfur, copper, gold and other chalcophile elements (e.g., Keith et al., 1997; Halter et al., 2002b, 2005; Stavast et al., 2006), and magmatic amphiboles and biotites commonly are replaced by secondary biotite and/or chlorite. Subsolidus oxidation and minor alteration of the upper part of the uranium and base-metal mineralized Eibenstock Granite, Germany, correlates with a decrease in S, U, Th, Pb, Zn, Cu, Sn, W and As in the whole rock, and it was argued that the missing amount of metals in the altered rocks could easily make up the mass of metals found in the ore deposit (Barsukov et al., 2006). In contrast, a study of mafic minerals in barren and mineralized porphyries indicates that the copper content of chlorite and secondary biotite is higher than that of their magmatic precursor minerals (Graybeal, 1973; Hendry et al., 1985). Thus, it remains to be determined whether this stage promotes or diminishes the mineralization potential. However, the process is expected to occur to similar degrees in both barren and mineralized plutons; thus, a major control on the mineralization potential appears unlikely.

Fluid focusing is a key process for magmatic-hydrothermal ore formation because economic mineralization can only form if relatively large volumes of fluid precipitate metals in a comparatively small rock volume. The locally mineralized but economically barren intrusions at Cuasso al Monte, Mt. Malosa and Baveno are impressive testimonies to this principle. Fluid focusing acts at all scales ranging from the formation of kilometer-sized apophyses into which residual melts and fluids are focused from large, underlying magma chambers, to millimeter-sized cracks in a stockwork breccia that create permeability for increased fluid flow. There are few studies dealing with the influence of intrusion shape and the degree of fracturing on the mineralization potential. In a comparative study of barren and mineralized Laramide stocks in Arizona, Rehrig and Heidrick (1972) noted that the crucial structural difference which best contrasts ore-grade porphyries from the barren stocks is the intensity and complexity of the fine fractures. On the other hand, many intrusions associated with greisens and/or skarns developed only little veining, demonstrating that fracturing is not necessary for the formation of an ore deposit. More work needs to be done to fully assess the relative importance of this aspect. However, even if fluid focusing is crucial, it likely affects only the size and geometry of the deposit, not the deposit type.

Finally, the data in Table 2 demonstrate that a distinct correlation between ore type and fluid composition already exists in the single-phase parent fluids. Hence, even though selective metal precipitation and fluid immiscibility certainly had a significant impact on the composition of fluids under subsolidus conditions, a substantial proportion of the deposit-specific metal signature of magmatic fluids must have been acquired at an earlier stage (i.e., during the exsolution of fluids from crystallizing magmas and/or at an earlier stage).

8. Conclusions

Fluid inclusions provide a means of studying the fluids that are related to magmatic-hydrothermal ore deposits, and to examine the possible mechanisms leading to their formation. Provided that the inclusions are well preserved and that timing relationships with respect to the mineralization are well established, such inclusions can be used to address fundamental questions regarding the mineralization process.

In 10 out of the 17 magmatic systems considered in this study, the initially exsolved aqueous fluid was a single-phase of relatively low salinity (2-8 wt% $NaCl_{equiv}$). In four

occurrences (Cuasso al Monte, Mt. Malosa, Capitan Pluton, and Santa Rita), vapor and brine directly exsolved from the melt, whereas in the three remaining occurrences (Bajo de la Alumbrera, Grasberg and Cave Peak) the nature of the initially exsolved fluid phase(s) could not be determined. Due to the relatively low salinity of the magmatic bulk fluids, they intersect their solvus on the vapor-rich side, resulting in the condensation of small amounts of brine out of the low-density bulk fluids. These observations are in accord with models developed by Henley and McNabb (1978) and Burnham (1979), and with more recent studies on barren and mineralized systems (e.g., Piccoli and Candela, 1994; Stix and Layne, 1996; Gerlach et al., 1996; Rusk et al., 2004; Redmond et al., 2004; Landtwing et al., 2005; Klemm et al., 2007; Zajacz et al., 2008). Depending on the depth of magma crystallization (i.e., confining pressure), the salinity of the bulk fluid either decreased (P >1.3 kbar) or increased (P <1.3 kbar) with increasing degree of melt fractionation, as is predicted by numerical models of magma crystallization (e.g., Nakano and Urabe, 1989; Cline and Bodnar, 1991; Candela and Piccoli, 1998).

The metal content of magmatic, low-salinity fluids correlates positively with the type and amount of mineralization in the associated intrusions, with high Cu concentrations found in porphyry Cu deposits, high Sn and W concentrations found in the Sn-W-mineralized systems, and high Ce concentrations in REE-mineralized systems. This implies that a significant part of the geochemical signature of these deposits was determined during processes operating at the magmatic stage. In the case of Mo, Sn, W and Ce, the correlation between fluid composition and type and amount of mineralization is greater in high-temperature, pre-mineralization brines than in their low-salinity, parental fluids. This, together with other lines of evidence (a strong spatial and temporal relationship between locations of mineralization and areas in which brine inclusions are abundant; chemical evolution of brines in the veins of the Mole Granite) suggest that brines played a central role in the formation of Sn, W, Mo and REE deposits. If true, then the timing and duration of vapor-brine immiscibility may be a critical parameter in these systems. In the case of porphyry Cu (-Au) deposits, mass balance calculations suggests that a larger amount of metal is associated with the vapor phase; however, we cannot rule out the possibility that brines were involved to a significant degree as well. Early fluids found in barren intrusions are not particularly rich in any of the metals considered here, except for elevated concentrations of Mo, Sn, W and Ce in some of the fluids analyzed from Cuasso al Monte, Mt. Malosa and Baveno. These latter three localities are well known for a large variety of minerals (including cassiterite, wolframates, molybdates and REE-bearing minerals) occurring in miarolitic cavities, demonstrating that the fluids had the potential to produce mineralization but were not sufficiently focused to form an economic deposit. Selective metal precipitation occurred in all deposits, affecting metals of both major and minor concentration. However, the main role of such selective precipitation was likely to separate spatially, and possibly temporally, distal Pb, Zn and Ag mineralization from intrusion-proximal Cu, Mo, Sn, W, and REE mineralization, rather than to control the relative metal abundances in the ore system as a whole.

More broadly speaking, we now seem to be at a point where we are able to characterize the nature and metal content of magmatic-hydrothermal fluids. Thus, we should be on the edge of linking these observations to petrologic processes such as fractional crystallization or magma mixing, to investigate whether or not there are non-metal signatures indicative of the mineralization potential of a given intrusion. Future studies with strong emphasis on the integration of mapping, field relationships, petrographic characterization and chemical analysis at various scales will help to understand the connection between magmatic processes and the composition of magmatic-hydrothermal fluids.

Acknowledgments

References

Allen, M. S., and McLemore, V. T., 1991, The geology and petrogenesis of the Capitan Pluton, New Mexico, *in* Barker, J. M., Kues, B. S., Austin, G. S., and Lucas, S. G., eds., Fall field conference guidebook 42: Geology of the Sierra Blanca, Sacramento, and Capitan Ranges, New Mexico: Socorro, New Mexico Geological Society, p. 115-127.

Audétat, A., Günther, D., and Heinrich, C. A., 1998, Formation of a magmatic-hydrothermal ore deposit: Insights with LA-ICP-MS analysis of fluid inclusions: Science, v. 279, p. 2091-2094.

Audétat, A., and Günther, D., 1999, Mobility and H_2O-loss from fluid inclusions in natural quartz crystals: Contributions to Mineralogy and Petrology, v. 137, p. 1-14.

Audétat, A., Günther, D., and Heinrich, C. A., 2000a, Magmatic-hydrothermal evolution in a fractionating granite: A microchemical study of the Sn-W-F-mineralized Mole Granite (Australia): Geochimica et Cosmochimica Acta, v. 64, p. 3373-3393.

Audétat, A., Günther, D., and Heinrich, C. A., 2000b, Causes for large-scale metal zonation around mineralized plutons: Fluid inclusion LA-ICP-MS evidence from the Mole Granite, Australia: Economic Geology, v. 95, p. 1563-1581.

Audétat, A., and Pettke, T., 2003, The magmatic-hydrothermal evolution of two barren granites: a melt and fluid inclusion study of the Rito del Medio and Cañada Pinabete Plutons in northern New Mexico (USA): Geochimica et Cosmochimica Acta, v. 67, p. 97-121.

Audétat, A., Pettke, T., and Dolejs, D., 2004, Magmatic anhydrite and calcite in the ore-forming quartz-monzodiorite magma at Santa Rita, New Mexico (USA): genetic constraints on porphyry-Cu mineralization: Lithos, v. 72, p. 147-161.

Audétat, A., and Pettke, T., 2006, Evolution of a porphyry-Cu mineralized magma system at Santa Rita, New Mexico (U.S.A.): Journal of Petrology, v. 47, p. 2021-2046.

Barsukov, V. L., Sokolova, N. T., and Ivanitskii, O. M., 2006, Metals, arsenic and sulfur in the Aue and Eibenstock granites, Erzgebirge: Geochemistry International, v. 44, p. 896-911.

Baumann, L., Kuschka, E., and Seifert, T., 2000, Lagerstätten des Erzgebirges: Stuttgart, Germany, Enke, 300 p.

Bodnar, R. J., Burnham, C. W., and Sterner, S. M., 1985, Synthetic fluid inclusions in natural quartz. III. Determination of phase equilibrium properties in the system H_2O-NaCl to 1000°C and 1500 bars: Geochimica et Cosmochimica Acta, v. 49, p. 1861-1873.

Bodnar, R. J., 1995, Fluid inclusion evidence for a magmatic source of metals in porphyry

copper deposits, *in* Thompson, J. F. H., ed., Magmas, fluids and ore deposition: Victoria, British Columbia, Mineralogical Association of Canada, Short Course Series, v. 23, p. 139-152.

Bodnar, R. J., and Student, J. J., 2006, Melt inclusions in plutonic rocks: Petrography and microthermometry, *in* Webster, J. D., ed., Melt inclusions in plutonic rocks, Mineralogical Association of Canada, Short Course Series, v. 36, p. 1-26.

Bowen, N. L., 1933, The broader story of magmatic differentiation, briefly told, *in* Finch, J. W., ed., Ore deposits of the Western States (Lindgren volume): New York, American Institute of Mining and Metallurgical Engineers, p. 106-128.

Burnham, C. W., 1967, Hydrothermal fluids at the magmatic stage, *in* Barnes, H. L., ed., Geochemistry of hydrothermal ore deposits, 1st edition: New York, Holt, Rinehart and Winston, p. 34-76.

Burnham, C. W., 1979, Magmas and hydrothermal fluids, *in* Barnes, H. L., ed., Geochemistry of hydrothermal ore deposits, 2nd edition: New York, Wiley, p. 71-136.

Burnham, C. W., 1997, Magmas and hydrothermal fluids, *in* Barnes, H. L., ed., Geochemistry of hydrothermal ore deposits, 3rd edition: New York, John Wiley & Sons, p. 63-124.

Campbell, A. R., 1995, The evolution of a magmatic fluid: A case history from the Capitan Mountains, New Mexico, *in* Thompson, J. F. H., ed., Magmas, fluids and ore deposits: Victoria, British Columbia, Mineralogical Association of Canada, v. 23, p. 291-308.

Campbell, A. R., Banks, D. A., Randall, S. P., and Yardley, B. W. D., 1995, Geochemistry of Th-U-REE mineralizing magmatic fluids, Capitan Mountains, New Mexico: Economic Geology, v. 90, p. 1271-1287.

Candela, P. A., 1989, Magmatic ore-forming fluids: Thermodynamic and mass transfer calculations of metal concentrations, *in* Whitney, J. A., and Naldrett, A. J., eds., Ore Deposition Associated with Magmas: Reviews in Economic Geology, v. 4, p. 203-221.

Candela, P. A., and Blevin, P. L., 1995, Do some miarolitic cavities preserve evidence of magmatic volatile phase permeability? Economic Geology, v. 90, p. 2310-2316.

Candela, P. A., and Holland, H. D., 1984, The partitioning of copper and molybdenum between silicate melts and aqueous fluids: Geochimica et Cosmochimica Acta, v. 48, p. 373-388.

Candela, P. A., 1989, Magmatic ore-forming fluids: thermodynamic and mass transfer calculations of metal concentrations, *in* Whitney, J. A., and Naldrett, A. J., eds., Ore Deposition Associated with Magmas: Reviews in Economic Geology, vol. 4, p. 203-221.

Candela, P. A., and Piccoli, P. M., 1995, Model ore-metal partitioning from melts into vapor and vapor/brine mixtures, *in* Thompson, J. F. H., ed., Magmas, Fluids and Ore Deposits: Victoria, British Columbia, Mineralogical Association of Canada, Short Course Series, v. 23, p. 101-127.

Candela, P. A., and Piccoli, P. M., 1998, Magmatic contributions to hydrothermal ore deposits: an algorithm (MVPart) for calculating the composition of the magmatic volatile phase, *in* Richardson, J., and Larsen, P., eds., Techniques in Hydrothermal

Ore Deposit Geology: Reviews in Economic Geology, v. 10, p. 97-108.

Cathles, L. M., 1981, Fluid flow and genesis of hydrothermal ore deposits: Economic Geology 75th Anniversary Volume, p. 424-457.

Christiansen, E. H., Burt, D. M., Sheridan, M. F., and Wilson, R. T., 1983, The petrogenesis of topaz rhyolites from the Western United States: Contributions to Mineralogy and Petrology, v. 83, p. 16-30.

Clark, K. F., and Read, C., 1972, Geology and ore deposits of the Eagle Nest area, New Mexico, New Mexico Bureau of Geology and Mineral Resources Bulletin 94, 152 p.

Cline, J. S., and Bodnar, R. J., 1991, Can economic porphyry copper mineralization be generated by a typical calc-alkaline melt?: Journal of Geophysical Research, v. 96, p. 8113-8126.

Demartin, F., Guastoni, A., Pezzotta, F., and Picciani, M., 2003, Neufunde aus den Pegmatiten Zomba-Malosa, Malawi: Lapis, v. 28, p. 18-21.

Drewes, H., 1987, Geologic map and cross sections of the Dragoon Mountains, southeastern Arizona: U.S. Geological Survey Miscellaneous investigations series, Map I-1662.

Drummond, S. E., and Ohmoto, H., 1985, Chemical evolution and mineral deposition in boiling hydrothermal systems: Economic Geology, v. 87, p. 1963-2001.

Eadington, P. J., 1983, A fluid inclusion investigation of ore formation in a tin-mineralized granite, New England, New South Wales: Economic Geology, v. 78, p. 1204-1221.

Eastoe, C. J., 1982, Physics and chemistry of the hydrothermal system at the Panguna porphyry copper deposit, Bougainville, Papua New Guinea: Economic Geology, v. 77, p. 127-153.

Emmons, W. H., 1933, On the mechanism of the deposition of certain metalliferous lode systems associated with granitic batholiths, *in* Finch, J. W., ed., Ore deposits of the Western States (Lindgren volume): New York, American Institute of Mining and Metallurgical Engineers, p. 327-349.

Fenner, C. N., 1933, Pneumatolytic processes in the formation of minerals and ores, *in* Finch, J. W., ed., Ore deposits of the Western States (Lindgren volume): New York, American Institute of Mining and Metallurgical Engineers, p. 58-106.

Gerlach, T. M., Westrich, H. R., and Symonds, R. B., 1996, Preeruption vapor in the magma of the climactic Mount Pinatubo eruption: source of the giant stratospheric sulfur dioxide cloud, *in* Newhall, C. G., and Punongbayan, R. S., eds., Fire and mud: eruption and lahars of the Mount Pinatubo, Philippines: Seattle, Univ. Washington Press, p. 415-433.

Gilluly, J., 1956, General geology of Central Cochise County, Arizona: U.S. Geological Survey, Professional Paper 281, 169 p.

Goldstein, R. H., and Reynolds, T. J., 1994, Systematics of fluid inclusions in diagenetic minerals: Tulsa, Oklahoma, Society for Sedimentary Geology, 199 p.

Graybeal, F. T., 1973, Copper, manganese, and zinc in coexisting mafic minerals from Laramide intrusive rocks in Arizona: Economic Geology, v. 68, p. 785-798.

Guastoni, A., Demartin, F., and Pezzotta, F., 2004, Mineralogische Neuigkeiten aus Zomba, Malawi: Genthelvin, Kainosit, Scheelit und Sphalerit: Lapis, v. 29, p. 37-38.

Günther, D., Audétat, A., Frischknecht, R., and Heinrich, C. A., 1998, Quantitative analysis of major, minor and trace elements in fluid inclusions using Laser Ablation-Inductively Coupled Plasma-Mass Spectrometry (LA-ICP-MS): Journal of Analytical Atomic Spectrometry, v. 13, p. 263-270.

Halter, W. E., Pettke, T., Heinrich, C. A., and Roth-Rutishauser, B., 2002a, Major to trace element analysis of melt inclusions by laser-ablation ICP-MS: methods of quantification: Chemical Geology, v. 183, p. 63-86.

Halter, W. E., Pettke, T., and Heinrich, C. A., 2002b, The origin of Cu/Au-ratios in porphyry-type ore deposits: Science, v. 296, p. 1844-1846.

Halter, W. E., Heinrich, C. A., and Pettke, T., 2005, Magma evolution and the formation of porphyry Cu-Au ore fluids: evidence from silicate and sulfide melt inclusions: Mineralium Deposita, v. 39, p. 845-863.

Hedenquist, J. W., and Lowenstern, J. B., 1994, The role of magmas in the formation of hydrothermal ore deposits: Nature, v. 370, p. 519-527.

Hedenquist, J. W., 1995, The ascent of magmatic fluids: Eruption versus mineralization, *in* Thompson, J. F. H., ed., Magmas, fluids and ore deposits, Mineralogical Association of Canada, Short course series, v. 23, p. 263-289.

Hedenquist, J. W., and Richards, J. P., 1998, The influence of geochemical techniques on the development of genetic models for porphyry copper deposits, *in* Richards, J. P., and Larson, P. B., eds., Techniques in Hydrothermal Ore Deposits Geology: Reviews in Economic Geology, v. 10, p. 235-256.

Hedenquist, J. W., Simmons, S. F., Giggenbach, W. F., and Eldridge, C. S., 1993, White Island volcanic hydrothermal system as an active analogue of the environment of high sulfidation Cu and Au ore deposition: Geology, v. 21, p. 731-734.

Hedenquist, J. W., Arribas, A., and Reynolds, T. J., 1998, Evolution of an intrusion-centered hydrothermal system: Far Southeast-Lepanto porphyry and epithermal Cu-Au deposits, Philippines: Economic Geology, v. 93, p. 373-404.

Heinrich, C. A., Günther, D., Audétat, A., Ulrich, T., and Frischknecht, R., 1999, Metal fractionation between magmatic brine and vapor, determined by microanalysis of fluid inclusions: Geology, v. 27, p. 755-758.

Heinrich, C. A., Pettke, T., Halter, W., Aigner-Torres, M., Audétat, A., Günther, D., Hattendorf, B., Bleiner, D., Guillong, M., and Horn, I., 2003, Quantitative multi-element analysis of minerals, fluid and melt inclusions by laser-ablation inductively-coupled-plasma mass-spectrometry: Geochimica et Cosmochimica Acta, v. 67, p. 3473-3496.

Heinrich, C. A., Driesner, T., Stefánsson, A., and Seward, T. M., 2004, Magmatic vapor contraction and the transport of gold from the porphyry environment to epithermal deposits: Geology, v. 32, p. 761-764.

Heinrich, C. A., 2005, The physical and chemical evolution of low- to medium-salinity magmatic fluids at the porphyry to epithermal transition: A thermodynamic study: Mineralium Deposita, v. 39, p. 864-889.

Hendry, D. A. F., Chivas, A. R., Long, J. V. P., and Reed, S. J. B., 1985, Chemical differences between minerals from mineralizing and barren intrusions from some North American porphyry copper deposits: Contributions to Mineralogy and Petrology, v. 89, p. 317-329.

Henley, R. W., and McNabb, A., 1978, Magmatic vapor plumes and ground-water

interaction in porphyry copper emplacement: Economic Geology, v. 7, p. 1-20.

Henley, H. F., Brown, R. E., and Stroud, W. J., 1999, The Mole Granite – extent of mineralization and exploration potential, *in* Flood, P. G., ed., Regional Geology, Tectonics and Metallogenesis of the New England Orogen: Univ. of New England, p. 385-392.

Henley, H. F., Brown, R. E., and Brownlow, J. W., 2000, The Mole Tableland – geology and mineral occurrences 1:50 000 map, Geological Survey of New South Wales, Sydney.

Holland, H. D., 1972, Granites, solutions and base metal deposits: Economic Geology, v. 67, p. 281-301.

Ishihara, S., and Takenouchi, S., 1980, Granitic magmatism and related mineralization: Mining Geology Special Issue, 8, The Society of Mining Geologists of Japan, 247 p.

Jahns, R. H., 1982, Internal evolution of pegmatite bodies, *in* Cerny, P., ed., Granitic Pegmatites in Science and Industry: Mineralogical Association of Canada, Short Course Handbook, vol. 8, p. 293-327.

John, D. A., 1989, Geologic setting, depth of emplacement, and regional distribution of fluid inclusions in intrusions of the Central Wasatch Mountains, Utah: Economic Geology, v. 84, p. 386-409.

Johnson, C. M., Czamanske, G. K., and Lipman, P. W., 1989, Geochemistry of intrusive rocks associated with the Latir volcanic field, New Mexico, and contrasts between evolution of plutonic and volcanic rocks: Contributions to Mineralogy and Petrology, v. 103, p. 90-109.

Jones, D. M., 1990, Mid-Tertiary arcuate dikes and faults of the Rio Hondo-Red River drainages, Sangre de Cristo Mountains, New Mexico: a postulated outlying ring-fracture zone to the Miocene Questa caldera: New Mexico Geological Society, Guidebook to the 41st field conference, p. 365-368.

Jones, W. R., Hernon, R. M., and Moore, S. L., 1967, General geology of the Santa Rita quadrangle, Grant Country, New Mexico, U. S. Geological Survey Professional Paper 555, 144 p.

Keith, J. D., Whitney, J. A., Hattori, K., Ballantyne, G. H., Christiansen, E. H., Barr, D. L., Cannan, T. M., and Hook, C. J., 1997, The role of magmatic sulfides and mafic alkaline magmas in the Bingham and Tintic mining districts, Utah: Journal of Petrology, v. 38, p. 1679-1690.

Keith, S. B., 1973, Index of mining properties in Cochise County, Arizona: Arizona Bureau of Geology and Mineral Technology, Bulletin 187, 98 p.

Keppler, H., and Wyllie, P. J., 1991, Partitioning of Cu, Sn, Mo, W, U and Th between melt and aqueous fluid in the systems haplogranite-H_2O-HCl and haplogranite-H_2O-HF: Contributions to Mineralogy and Petrology, v. 109, p. 139-150.

Kesler, S. E., 1994, Mineral resources, economics and the environment: New York, McMillan, 391 p.

Kilinc, I. A., and Burnham, C. W., 1972, Partitioning of chloride between a silicate melt and a coexisting aqueous phase from 2 to 8 kilobars: Economic Geology, v. 67, p. 231-235.

Klemm, L., Pettke, T., and Heinrich, C. A., 2007, Hydrothermal evolution of the El Teniente

deposit, Chile: porphyry Cu-Mo ore deposition from low-salinity magmatic fluids: Economic Geology, v. 102, p. 1021-1045.

Klemm, L., Pettke, T., and Heinrich, C. A., 2008, Fluid source and magma evolution of the Questa porphyry Mo deposit, New Mexico, USA: Mineralium Deposita, v. 43, p. 533-552.

Kreidler, T. J., 1982, Mineral-resource potential of the Dragoon Mountains rare II further planning area, Cochise County, Arizona: U.S. Bureau of Mines Mineral Land Assessment, MLA 35-82.

Landtwing, M. R., Pettke, T., Halter, W. E., Heinrich, C. A., Redmond, P. B., Einaudi, M. T., and Kunze, K., 2005, Copper deposition during quartz dissolution by cooling magmatic-hydrothermal fluids: The Bingham porphyry: Earth and Planetary Science Letters, v. 235, p. 229-243.

Lindgren, W., 1905, The copper deposits of the Clifton-Morenci district, Arizona: U.S. Geological Survey Professional Paper, v. 43, p. pp. 375.

Long, K. R., 1992, Reserves and production data for selected ore deposits in the United States found in the files of the Anaconda Copper Company: U.S. Geological Survey Open-File Report 92-002, 21 p.

Lowell, J. D., and Guilbert, J. M., 1970, Lateral and vertical alteration-mineralization zoning in porphyry ore deposits: Economic Geology, v. 65, p. 373-408.

Luth, W. C., Jahns, R. H., and Tuttle, O. F., 1964, The granite system at pressures of 4 to 10 kbars: Journal of Geophysical Research, v. 69, p. 759-773.

McLemore, V. T., and Phillips, R. S., 1991, Geology of mineralization and associated alteration in the Capitan Mountains, Lincoln County, New Mexico, *in* Barker, J. M., Kues, B. S., Austin, G. S., and Lucas, S. G., eds., Fall field conference guidebook, v. 42: Geology of the Sierra Blanca, Sacramento, and Capitan Ranges, New Mexico: Socorro, New Mexico Geological Society, p. 291-298.

Moore, W. J., and Nash, J. T., 1974, Alteration and fluid inclusion studies of the porphyry-Cu ore body at Bingham, Utah: Economic Geology, v. 69, p. 631-645.

Muntean, J. L., and Einaudi, M. T., 2000, Porphyry gold deposits of the Refugio district, Maricunga belt, northern Chile: Economic Geology, v. 95, p. 1445-1472.

Mutschler, F. E., Ludington, S., and Bookstrom, A. A., 1999, Giant porphyry-related metal camps of the world - a database: U.S. Geological Survey Open-File Report 99-556,

Nakano, T., and Urabe, T., 1989, Calculated compositions of fluids released from a crystallizing granitic melt: importance of pressure on the genesis of ore forming fluid: Geochemical Journal, v. 23, p. 307-319.

Nielsen, R. L., 1968, Hypogene texture and mineral zoning in a copper-bearing granodiorite porphyry stock, Santa Rita, New Mexico: Economic Geology, v. 63, p. 37-50.

Norton, D. L., 1982, Fluid and heat transport phenomena typical of copper-bearing pluton environments, *in* Titley, S. R., ed., Advances in the Geology of Porphyry Copper Deposits of southwestern North America: Tucson, University of Arizona Press, p. 59-72.

Pettke T., Heinrich C. A., Ciocan A. C., and Günther D., 2000, Quadrupole mass spectrometry and optical emission spectroscopy: detection capabilities and representative sampling of short transient signals from laser-ablation. Journal of Analytical Atomic Spectrometry, v. 15, 1149-1155.

Pettke, T., 2006, In situ Laser-ablation-ICP-MS chemical analysis of melt inclusions and prospects for constraining subduction zone magmatism, *in* Webster, J. D., ed., Melt Inclusions in Plutonic Rocks: Mineralogical Association of Canada, Short Course Series, v. 36, p. 51-80.

Pezzotta, F., Diella, V., and Guastoni, A., 1999, Chemical and paragenetic data on gadolinite-group minerals from Baveno and Cuasso al Monte, southern Alps, Italy: American Mineralogist, v. 84, p. 782-789.

Piccoli, P., and Candela, P., 1994, Apatite in felsic rocks: a model for the estimation of initial halogen concentrations in the Bishop Tuff (Long Valley) and Toulumne Intrusive Suite (Sierra Nevada Batholith) magmas: American Journal of Science, v. 294, p. 92-135.

Piwinskii, A. J., and Wyllie, P. J., 1970, Experimental studies of igneous rock series: felsic body suite from the Needle Point Pluton, Wallowa Batholith, Oregon: Journal of Geology, v. 78, p. 52-76.

Plimer, I. R., Lu, J., Foster, D., and Kleeman, J. D., 1995, Ar-Ar dating of multiphase mineralization associated with the Mole Granite, Australia, *in* Pasava, J., Kribek, B., and Zak, K., eds., Mineral Deposits: From Their Origin to Their Environmental Impacts: Rotterdam, Balkema, p. 497-501.

Pollard, P. J., and Taylor, R. G., 2002, Paragenesis of the Grasberg Cu-Au deposit, Irian Jaya, Indonesia: results from logging section 13: Mineralium Deposita, v. 37, p. 117-136.

Ratajeski, K., and Campbell, A. R., 1994, Distribution of fluid inclusions in igneous quartz of the Capitan pluton, New Mexico, USA: Geochimica et Cosmochimica Acta, v. 58, p. 1161-1174.

Redmond, P. B., Einaudi, M. T., Inan, E. E., Landtwing, M. R., and Heinrich, C. A., 2004, Copper deposition by fluid cooling in intrusion-centered systems: New insights from the Bingham porphyry ore deposits, Utah: Geology, v. 32, p. 217-220.

Rehrig, W. A., and Heidrick, R. L., 1972, Regional fracturing in Laramide stocks of Arizona and its relationship to porphyry copper mineralization: Economic Geology, v. 67, p. 198-213.

Reynolds, T. J., and Beane, R. E., 1985, Evolution of hydrothermal fluid characteristics at the Santa Rita, New Mexico, porphyry-Cu deposit: Economic Geology, v. 80, p. 1328-1347.

Rickers, K., Thomas, R., and Heinrich, W., 2006, The behavior of trace elements during the chemical evolution of the H_2O-, B-, and F-rich granite-pegmatite-hydrothermal system at Ehrenfriedersdorf, Germany: a SXRF study of melt and fluid inclusions: Mineralium Deposita, v. 41, p. 229-245.

Robb, L., 2005, Introduction to ore-forming processes, Blackwell Publishing, Oxford, 373 p.

Roberts, S. A., 1975, Early hydrothermal alteration and mineralization in the Butte district, Montana: Unpublished PhD thesis, Harvard University, 157 p.

Roedder, E., 1971, Fluid inclusion studies on the porphyry-type ore deposits at Bingham, Utah, Butte, Montana, and Climax, Colorado: Economic Geology, v. 66, p. 98-120.

Roedder, E., 1984, Fluid inclusions: Washington DC, Reviews in Mineralogy, Mineralogical Society of America, vol. 12, 644 p.

Roedder, E., and Bodnar, R. J., 1997, Fluid inclusion studies of hydrothermal ore deposits. *in* Barnes, H. L., ed., Geochemistry of Hydrothermal Ore Deposits, 3rd ed.: Wiley and Sons Inc., New York, p. 857-698.

Rose, A. W., and Baltosser, W. W., 1966, The porphyry copper deposit at Santa Rita, New Mexico, *in* Titley, S. R., and Hicks, C. L., eds., Geology of the Porphyry Copper Deposits in Southwestern North America: University of Arizona, p. 205-220.

Rusk, B. G., Reed, M. H., Dilles, J. H., Klemm, L. M., and Heinrich, C. A., 2004, Compositions of magmatic hydrothermal fluids determined by LA-ICP-MS of fluid inclusions from the porphyry copper-molybdenum deposit at Butte, MT: Chemical Geology, v. 210, p. 173-199.

Seward, T. M., and Barnes, H. L., 1997, Metals transport by hydrothermal ore fluids, *in* Barnes, H. L., ed., Geochemistry of hydrothermal ore deposits: New York, Wiley, p. 435-477.

Sharp, J. E., 1979, Cave Peak, a Molybdenum-mineralized breccia pipe complex in Culberson County, Texas: Economic Geology, v. 74, p. 517-534.

Sheppard, S. M. F., Nielsen, R. L., and Taylor, H. P. J., 1971, Hydrogen and oxygen isotope ratios in minerals from porphyry copper deposits: Economic Geology, v. 66, p. 515-542.

Shinohara, H., Iiyama, J. T., and Matsuo, S., 1989, Partition of chlorine compounds between silicate melt and hydrothermal solutions, I partition of NaCl-KCl: Geochimica et Cosmochimica Acta, v. 53, p. 2617-2630.

Shinohara, H., 1994, Exsolution of immiscible vapor and liquid phases from a crystallizing silicate melt: Implications for chlorine and metal transport: Contributions to Mineralogy and Petrology, v. 58, p. 5215-5221.

Shinohara, H., and Hedenquist, J. W., 1997, Constraints on magma degassing beneath the Far Southeast porphyry Cu-Au deposit, Philippines: Journal of Petrology, v. 38, p. 1741-1752.

Stavast, W. J. A., Keith, J. D., Christiansen, E. H., Dorais, M. J., Larocque, A., and Evans, N., 2006, The fate of magmatic sulfides during intrusion or eruption, Bingham and Tintic Districts, Utah: Economic Geology, v. 101, p. 329-345.

Stein, H. J., and Hannah, J. L., 1990, Ore-bearing Granite Systems: Boulder, Colorado, Geological Society of America, Special Papers, 364 p.

Stix, J., and Layne, G., 1996, Gas saturation and evolution of volatile and light lithophile elements in the Bandelier magma chamber between two caldera-forming eruptions: Journal of Geophysical Research, v. 101(B11), pp. 25181-25196.

Sun, S. S., and Eadington, P. J., 1987, Oxygen isotope evidence for the mixing of magmatic and meteoric waters during tin mineralization in the Mole Granite, New South Wales, Australia: Economic Geology, v. 82, p. 43-52.

Taylor, H. P. J., 1974, The application of oxygen and hydrogen isotope studies to problems

of hydrothermal alteration and ore deposition: Economic Geology, v. 69, p. 843-883.

Taylor, R. P., and Strong, D. F., 1988, Recent advances in the geology of granite-related mineral deposits: Canadian Institute of Mining and Metallurgy, Special Volume, v. 39, 445 p.

Tuttle, O. F., and Bowen, N. L., 1958, Origin of granite in the light of experimental studies in the system $NaAlSi_3O_8-SKAlSi_3O_8-SiO_2-H_2O$: Geological Society of America Memoirs, v. 74, 153 p.

Uchida, E., Endo, S., and Makino, M., 2007, Relationship between solidification depth of granitic rocks and formation of hydrothermal ore deposits: Resource Geology, v. 57, p. 47-56.

Ulrich, T., Günther, D., and Heinrich, C. A., 2002, The evolution of a porphyry Cu-Au deposit, based on LA-ICP-MS analysis of fluid inclusions: Bajo de la Alumbrera, Argentina: Economic Geology, v. 97, p. 1889-1920.

Urabe, T., 1985, The effect of pressure on the partitioning ratios of lead and zinc between vapor and rhyolite melt: Economic Geology, v. 82, p. 1049-1052.

Webster, J. D., Holloway, J. R., and Hervig, R. L., 1989, Partitioning of lithophile trace elements between H_2O and H_2O+CO_2 fluids and topaz rhyolite melts: Economic Geology, v. 84, p. 116-134.

Webster, J. D., 1992, Fluid-melt interactions involving Cl-rich granites: Experimental study from 2 to 8 kbar: Geochimica et Cosmochimica Acta, v. 56, p. 659-678.

Webster, J. D., and Mandeville, C. W., 2007, Fluid immiscibility in volcanic environments, *in* Liebscher, A., and Heinrich, C. A., eds., Fluid-fluid interactions: Reviews in Mineralogy and Geochemistry, Mineralogical Society of America, v. 65, p. 313-362.

Whitney, J., and Naldrett, A. J., 1989, Ore Deposition Associated with Magmas: Reviews in Economic Geology, v. 4, 250 p.

Williams-Jones, A. E., and Heinrich, C. A., 2005, Vapor transport of metals and the formation of magmatic-hydrothermal ore deposits: Economic Geology, v. 100, p. 1287-1312.

Zajacz, Z., Halter, W. E., Pettke, T., and Guillong, M., 2008, Determination of fluid/melt partition coefficients by LA-ICPMS analysis of co-existing fluid and silicate melt inclusions: Controls on element partitioning: Geochimica et Cosmochimica Acta, v. 72, p. 2169-2197.